BULLETIN OF
MATHEMATICAL BIOLOGY
VOLUME 37 1975

BIFURCATION ANALYSIS OF NONLINEAR REACTION-DIFFUSION EQUATIONS—II. STEADY STATE SOLUTIONS AND COMPARISON WITH NUMERICAL SIMULATIONS

■ M. HERSCHKOWITZ-KAUFMAN
Faculté des Sciences,
Université Libre de Bruxelles
Belgium

The steady state spatial patterns arising in nonlinear reaction–diffusion systems beyond an instability point of the thermodynamic branch are studied on a simple model network. A detailed comparison between the analytical solutions of the kinetic equations, obtained by bifurcation theory, and the results of computer simulations is presented for different boundary conditions. The characteristics of the dissipative structures are discussed and it is shown that the observed behavior depends strongly on both the boundary and initial conditions. The theoretical expressions are limited to the neighborhood of the marginal stability point. Computer simulations allow not only the verification of their predictions but also the investigation of the behavior of the system for larger deviations from the instability point. It is shown that new features such as multiplicity of solutions and secondary bifurcations can appear in this region.

INTRODUCTION

It is well-known that for open chemical systems governed by nonlinear rate equations and coupled to transport processes such as diffusion, the stability of steady states far from equilibrium is not automatically ensured (Glansdorff and Prigogine, 1971; Perlmutter, 1972).

Hence, beyond a critical distance from thermodynamic equilibrium such systems may become unstable and undergo a complete change of their macroscopic properties with respect to those on the *thermodynamic branch*, which corresponds to the extrapolation of the close-to-equilibrium behavior.

A great diversity of phenomena may occur beyond instability. It has been shown that the new regimes may correspond to temporally, spatially or even spatio-temporally organized states (Turing, 1952; Prigogine, 1969; Prigogine and Nicolis, 1971; Nicolis and Portnow, 1973). Because they spontaneously appear in response to a large deviation from thermodynamic equilibrium these states have been called 'dissipative structures' by Prigogine *et al.* (1969). It is interesting to note that the conditions required for the appearance of these dissipative structures are realized in numerous biological processes and the implications of these non-equilibrium order phenomena for certain fundamental biological problems have been emphasized.

Experimental examples of dissipative structures are known for both biological and non-biological chemical networks. Let us mention some systems which are at present of much interest: the glycolytic cycle (Chance *et al.*, 1973; Goldbeter and Lefever, 1972) and the Belousov–Zhabotinski reaction (Noyes *et al.*, 1972). The latter presents a great variety of organized patterns (Winfree, 1974). The general ideas underlying the theory of dissipative structures have been illustrated on a simple model system involving the following set of coupled chemical reactions:

$$\begin{aligned} A &\rightleftharpoons X && \text{(a)} \\ 2X + Y &\rightleftharpoons 3X && \text{(b)} \\ B + X &\rightleftharpoons Y + D && \text{(c)} \\ X &\rightleftharpoons E && \text{(d)} \end{aligned} \qquad (1.1)$$

the system is open to the initial and final chemicals A, B, D and E, whose concentrations are imposed throughout the system;

nonlinearity is introduced by the auto- and cross-catalytic steps (b) and (c);

the autocatalytic step (b) corresponds to a trimolecular reaction. Hanusse (1972) and Tyson (1973, 1974) have shown that for a reaction chain with only two intermediate species this is the simplest nonlinearity compatible with the law of mass action, capable of leading to an instability of the thermodynamic branch.

Scheme (1.1) has thus to be considered as a minimal theoretical model exhibiting cooperative behavior.

In this paper, we analyze some properties of the dissipative structures arising in nonlinear reaction–diffusion systems, within the framework of this model. For simplicity, we set all forward kinetic constants equal to unity. The inverse reaction rates are neglected: the system is thus automatically operating at an

infinite distance from thermodynamic equilibrium. Assuming a bounded, one-dimensional medium, the rate equations describing (1.1) are:

$$\begin{aligned} \frac{\partial X}{\partial t} &= A + X^2Y - (B + 1)X + D_X \cdot \frac{\partial^2 X}{\partial r^2} \\ \frac{\partial Y}{\partial t} &= BX - X^2Y + D_Y \cdot \frac{\partial^2 Y}{\partial r^2} \quad (0 \leqslant r \leqslant L). \end{aligned} \tag{1.2}$$

where D_X and D_Y are the diffusion coefficients of X and Y assuming that Fick's law is valid.

Two types of boundary conditions will be considered:

1. Zero flux boundary conditions (Neumann conditions):

$$\frac{\partial}{\partial r} X(0, t) = \frac{\partial}{\partial r} X(L, t) = \frac{\partial}{\partial r} Y(0, t) = \frac{\partial}{\partial r} Y(L, t) = 0 \quad (t \geqslant 0). \tag{1.3}$$

2. Fixed boundary conditions (Dirichlet conditions):

$$\begin{aligned} X(0, t) &= X(L, t) = A \\ Y(0, t) &= Y(L, t) = B/A \quad (t \geqslant 0). \end{aligned} \tag{1.4}$$

When A and B are maintained constant in time and space, previous studies have shown that:

there is a unique uniform steady state solution:

$$X_0 = A, \qquad Y_0 = B/A \tag{1.5}$$

which is the continuation of the close to equilibrium behavior. For certain sets of values of the system's parameters A, B, D_X and D_Y, (1.5) becomes unstable. Beyond instability the system evolves either to new space-dependent steady states or to time-periodic regimes.

This paper is devoted to the study of steady state dissipative structures. For, if the existence of uniform limit cycle oscillations in chemical systems is now firmly established both experimentally and theoretically (Nicolis and Portnow, 1973; Noyes and Field, 1974), experimental evidence for steady state patterns is much less obvious (Kopell and Howard, 1973). In biology, spatial ordering is often associated with the existence of structures like membranes, although the biological importance of the emergence of order in a previously structureless medium has been recognized. The mechanisms of spontaneous pattern formation and its detailed properties however, have not yet been studied on a theoretical basis comparable to that of limit cycles, and it is therefore interesting to establish more rigorously the existence of symmetry-breaking transitions induced by diffusion.

The formulation presented in this paper concerns bounded media for which a clear distinction exists between transient behavior and the asymptotic states arising for long times which interest us. Furthermore, in chemistry and biology the boundaries of the system often play a very important role in the evolution of the system.

The role of diffusion in self-organization will be studied analytically and by computer simulation. First it will be seen that many of the different patterns which are found by numerical integration (Herschkowitz-Kaufman, 1973) can be analyzed in the framework of a very simple bifurcation scheme. However, the theory of nonlinear parabolic partial differential equations is much less developed than the theory of ordinary differential equations. Computer simulations allow us to investigate a greater diversity of situations, providing guide for further theoretical developments.

In Section II, we consider the case where A is distributed uniformly. We first summarize the results of the linear stability analysis of the thermodynamic branch (1.5) for both fixed and zero flux boundary conditions and present some typical stability diagrams.

We then study the nature of the new steady state solutions appearing beyond instability. Their particular qualitative and quantitative properties are discussed and we will see that the observed behavior depends strongly on both the boundary and initial conditions.

Mathematically, the transition to new steady state configurations can be understood as a phenomenon of branching of solutions of nonlinear partial differential equations (Sattinger, 1973). In a preceding paper Auchmuty and Nicolis (1975) developed a theoretical analysis of the equations (1.2) using bifurcation theory. A systematic perturbation scheme was introduced which allows the analytical calculation of the form of the bifurcating steady state in the neighborhood of the marginal stability point. The analytical expressions constructed by Nicolis and Auchmuty apply to the particular case of fixed boundary conditions (Dirichlet conditions). Using the same perturbation technique, we will perform the theoretical calculations for the case of zero flux boundary conditions (Neumann conditions) and analyze the influence of the boundary conditions on the characteristics of the bifurcating dissipative structures.

We also study the behavior of the system in the unstable region for different boundary and initial conditions by direct numerical integration of the nonlinear equations (1.2) on a digital computer. The results of computer simulation are compared with the theoretical predictions for both fixed and zero flux boundary conditions. The theoretical expressions, however, are limited to the neighborhood of the instability point. Computer simulations allow the verifi-

cation of their predictions and also the investigation of the behavior of the system for larger deviations from the marginal point. We shall see that new features arise in these regions.

In Section III, we analyze the case where the condition of uniform distribution of A is suppressed. It is shown that the uniform steady states which appear may now correspond to localized dissipative structures. The results of computer simulation are compared with the theoretical analysis of the localization of dissipative structures in terms of turning points presented by Auchmuty and Nicolis (1975).

II. STEADY STATE DISSIPATIVE STRUCTURES IN UNIFORM MEDIA

1. Linear Stability Analysis

In this section we present a summary with numerical results for the linear stability analysis of the uniform steady state (1.5) taking into account the two kinds of boundary conditions (1.3) and (1.4). We are essentially interested in establishing a stability diagram which will provide some insight in the type of solution to be expected beyond instability.

Thus, setting in (1.2):

$$\begin{aligned} X(r, t) &= X_0(r) + x(r, t) \\ Y(r, t) &= Y_0(r) + y(r, t) \end{aligned} \tag{2.1}$$

with

$$\left|\frac{x}{X_0}\right| \ll 1 \qquad \left|\frac{y}{Y_0}\right| \ll 1$$

we obtain the following linearized equations for the perturbations x and y:

$$\frac{\partial x}{\partial t} = (B - 1)x + A^2 y + D_X \cdot \frac{\partial^2 x}{\partial r^2} \tag{2.2}$$

$$\frac{\partial y}{\partial t} = -Bx - A^2 y + D_Y \cdot \frac{\partial^2 y}{\partial r^2} \quad (0 \leqslant r \leqslant L)$$

together with the alternative boundary conditions:

$$x(0, t) = x(L, t) = y(0, t) = y(L, t) = 0 \quad \text{(fixed B.C.)} \tag{2.3a}$$

$$\frac{\partial}{\partial r} x(0, t) = \frac{\partial}{\partial r} x(L, t) = \frac{\partial}{\partial r} y(0, t) = \frac{\partial}{\partial r} y(L, t) = 0 \quad \text{(zero flux B.C.).} \tag{2.3b}$$

The time dependence of the solution of (2.2)–(2.3) is of the form $e^{w_n t}$ where w_n,

which may be a complex quantity, corresponds to the eigenvalues of the operator $\mathscr{L}$ defined as

$$\mathscr{L} \equiv \begin{pmatrix} D_X \cdot \dfrac{d^2}{dr^2} + B - 1 & A^2 \\ -B & D_Y \cdot \dfrac{d^2}{dr^2} - A^2 \end{pmatrix}. \tag{2.4}$$

Its eigenfunctions must satisfy the prescribed boundary conditions. Hence the solution of (2.2) will be given by:

For fixed boundary conditions

$$\begin{pmatrix} x \\ y \end{pmatrix} = \begin{pmatrix} c_1 \\ c_2 \end{pmatrix} e^{w_n t} \sin \frac{n\pi r}{L} \quad (n = 1, 2, 3 \ldots) \tag{2.5a}$$

For zero flux boundary conditions

$$\begin{pmatrix} x \\ y \end{pmatrix} = \begin{pmatrix} c_1 \\ c_2 \end{pmatrix} e^{w_n t} \cos \frac{n\pi r}{L} \quad (n = 0, 1, 2, 3 \ldots). \tag{2.5b}$$

Inserting one of the expressions (2.5) into (2.2) one is led to the *secular equation* relating w_n to the wave number n and the system's parameters:

$$w_n^2 - \mathrm{Tr}\, w_n + \Delta = 0 \tag{2.6}$$

where

$$\mathrm{Tr} = B - (A^2 + 1) - \beta(D_X + D_Y)$$
$$\Delta = A^2 + \beta[A^2 D_X + (1 - B)D_Y] + \beta^2 D_X D_Y$$

and

$$\beta = \left(\frac{n\pi}{L}\right)^2.$$

Instability of the thermodynamic branch will occur for some value of n, if at least one of the roots of (2.6) has a positive real part. The main point is thus to establish the conditions for marginal stability, Re $w_n = 0$, corresponding either to 'exchange of stability', Im $w_n = 0$, or to 'overstability' Im $w_n \neq 0$.
A close analysis of (2.6) shows that:

(a) *the values of w_n are complex if:*

$$(A - \delta^{1/2})^2 < B < (A + \delta^{1/2})^2 \tag{2.7}$$

where $\delta = 1 - \beta(D_X - D_Y)$ must be a positive quantity. In this case marginal stability occurs at the critical point:

$$B = B_{1c}(n) = 1 + A^2 + \beta(D_X + D_Y). \tag{2.8}$$

One sees immediately that for impermeable boundaries the minimum value of (2.8) arises always for $n = 0$, while for fixed boundary conditions it corresponds to $n = 1$, zero being excluded by (2.5a).

Combining (2.7) and (2.8) it follows that the homogeneous steady state becomes unstable through complex eigenvalues of the operator $\mathscr{L}$ provided:

$$A^2 + 1 + \beta(D_X + D_Y) < B < A^2 + 1 + \beta(D_X - D_Y) + 2A[1 + \beta(D_X - D_Y)]^{1/2}. \quad (2.9)$$

(b) *the thermodynamic branch becomes unstable through real eigenvalues at the critical point of neutral stability:*

$$B = B_{2c}(n) = \frac{1}{\beta D_Y}(1 + \beta D_X)(A^2 + \beta D_Y). \quad (2.10)$$

For $B > B_{2c}(n)$, (1.5) corresponds to a saddle point, by definition unstable, while for $B < B_{2c}(n)$ the system is stable provided $\mathrm{Tr} < 0$.

The value of n minimizing (2.10) is now dependent on D_X, D_Y, A and L. Indeed, treating n as a continuous variable one obtains, by minimization:

$$n_{\min} = \frac{L}{\pi} \cdot \frac{A^{1/2}}{(D_X D_Y)^{1/4}} \quad (2.11)$$

$$B_{\min} = \left\{1 + A \cdot \left(\frac{D_X}{D_Y}\right)^{1/2}\right\}^2. \quad (2.12)$$

Accordingly, the critical wave number corresponding to onset of instability will be given by $n_{\min}$ if it is an integer or by one of the two closest integers.

For real w_n's the instability condition reads thus:

$$B \geqslant B(n_c) = \min_{\substack{n \geq 1 \\ \text{integer}}} \left\{1 + \frac{D_X}{D_Y} A^2 + \frac{A^2}{D_Y \beta} + \beta D_X\right\} \quad (2.13)$$

and applies for both kind of boundary conditions.

It is of interest to note that for certain sets of parameters there could be two critical wave numbers corresponding to a degenerate zero eigenvalue. We will however limit our study to the case where the eigenvalue $\mathrm{Re}\, w_n = 0$ is simple valued. The eigenfunction of $\mathscr{L}$ corresponding to the critical mode then has the form:

$$\begin{pmatrix} x^* \\ y^* \end{pmatrix} = \begin{pmatrix} c_1 \\ c_2 \end{pmatrix} \sin \frac{n_c \pi r}{L} \quad (2.14)$$

for fixed boundary conditions; for zero fluxes at the boundaries one gets instead:

$$\begin{pmatrix} x^* \\ y^* \end{pmatrix} = \begin{pmatrix} c_1 \\ c_2 \end{pmatrix} \cos \frac{n_c \pi r}{L}. \quad (2.15)$$

Substitution of these critical modes into the linear equations (2.2) taken at the steady state, leads to the following relation between c_1 and c_2 at the critical point:

$$\frac{c_2}{c_1} = \frac{D_X\beta + 1 - B_c}{A^2} \tag{2.16}$$

which becomes for B_c, n_c given by (2.11)–(2.12):

$$\frac{c_2}{c_1} = -\frac{1}{A}\left(\frac{D_X}{D_Y}\right)^{1/2}\left[1 + A\left(\frac{D_X}{D_Y}\right)^{1/2}\right]. \tag{2.17}$$

Which of the two neutral stability conditions (2.8) or (2.13) will be satisfied first as B increases from zero is determined, for given A and L, by the ratio of the diffusion coefficients. Two characteristic situations are illustrated in Figure 1

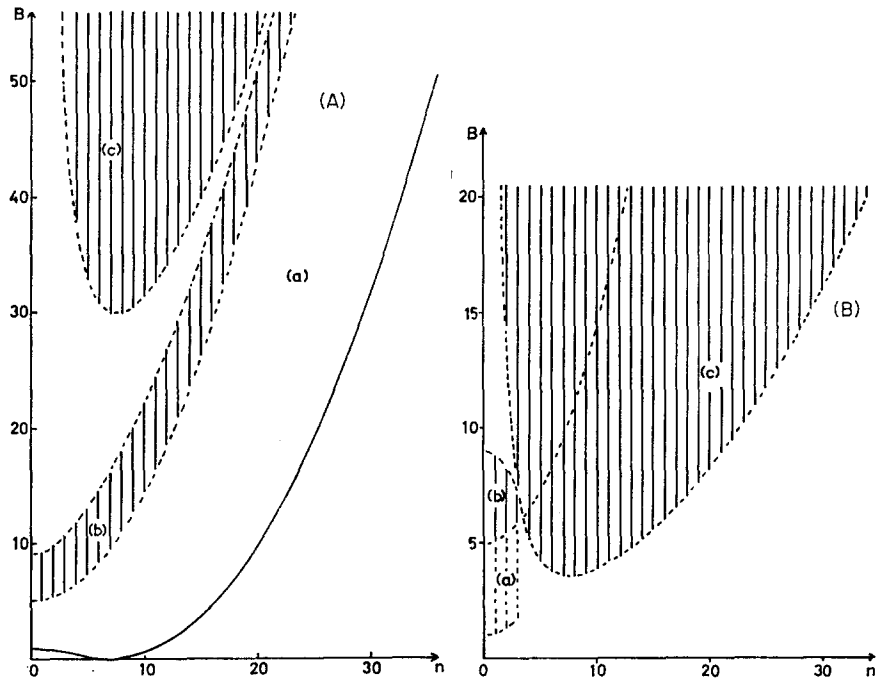

Figure 1. Linear stability diagrams resulting from equations (2.8)–(2.13). The bifurcation parameter B is plotted against the wave number n. (a) and (b) region of complex eigenvalues; (b) region corresponding to an unstable focus; (c) unstable region corresponding to a saddle point. The vertical lines indicate the allowed discrete values of n for a system submitted to zero fluxes or fixed boundary conditions. Figure 1A: $A = 2$, $L = 1$, $D_X = 8.0 \times 10^{-3}$, $D_Y = 1.6 \times 10^{-3}$. Figure 1B: $A = 2$, $L = 1$, $D_X = 1.6 \times 10^{-3}$, $D_Y = 8.0 \times 10^{-3}$

where the various relations (2.7)–(2.13) are represented graphically. They refer to both kinds of boundary conditions, having in mind that $n = 0$ is excluded for fixed concentrations at the boundaries. The curves $B(n)$ determine the discrete spectrum of null eigenvalues of operator $\mathscr{L}$.

In the first case (Figure 1A, $D_X/D_Y = 5$), instability arises first through complex eigenvalues: the new bifurcating solutions will be time periodic solutions of (1.2). They correspond either to standing waves, propagating waves or even to homogeneous limit cycle oscillations, depending on the parameters' values and boundary conditions. These types of solutions will be analyzed in detail in a forthcoming paper (see also Kopell and Howard, 1973; Ortoleva and Ross, 1974).

In the second case (Figure 1B, $D_X/D_Y = \frac{1}{5}$), the region of real roots is favored by the small ratio of D_X/D_Y. This corresponds to the bifurcation to new, non uniform, steady state solutions. The analytical and numerical results we shall report refer to this case. Figure 1B shows that as B is increased one passes successively through more and more unstable modes but the spacing between the values of B corresponding to the new null eigenvalues increases rapidly.

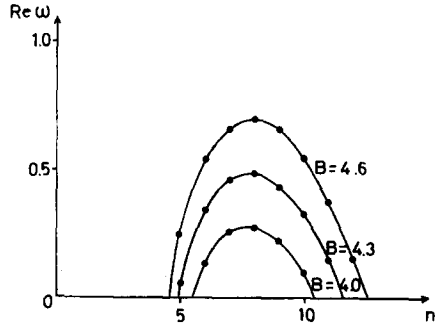

Figure 2. Real part of the eigenvalues w_n corresponding to the unstable modes emerging from the thermodynamic branch, for different values of B (zero fluxes and fixed boundary conditions). Numerical values used: $A = 2$, $L = 1$, $D_X = 1.6 \times 10^{-3}$, $D_Y = 8.0 \times 10^{-3}$

Moreover, one observes in Figure 2 that the first unstable mode corresponds to the eigenvalue with greatest real part or amplification factor. We shall see that the shape of the concentration profiles of the first bifurcating solution is closely related to the form of this critical mode and thus to the boundary conditions.

In this context, it is interesting to note that for two-dimensional systems, the geometry also plays an important role. The quantization of the different characteristics and resulting diversity of situations beyond instability then

become much more complex (Erneux and Herschkowitz-Kaufman, 1975). It should be pointed out that in the choice of the numerical values of the parameters, what matters is the ratio of the diffusion coefficients to the rate constants rather than the detailed values of these parameters. Moreover, the latter can be modified arbitrarily to more realistic values by changing the time and length scales.

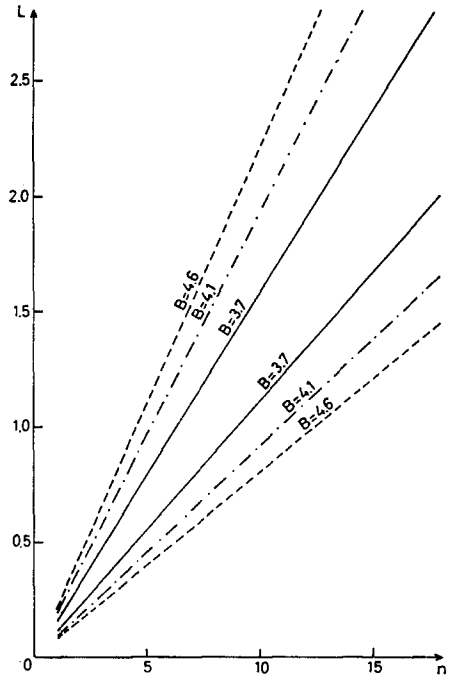

Figure 3. Instability through real eigenvalues in function of the size L of the system. For a given value of B the unstable region is delimited by two straight lines corresponding to the loci of the roots (L_0, L_1) of the equation $\Delta(1/L^2) = 0$. The numerical values of the various parameters are the same as in Figure 2

The effect of varying the size of the system can also be studied by analyzing (2.6). Indeed the coefficients of the characteristic equation can in particular be viewed as polynomials of $1/L^2$. As before there exist two possibilities for onset of instability: trough complex or real roots. In the latter case, for a given set of parameters, there will always be a minimum size, $L_{\min}$, corresponding to $n = 1$, below which the homogeneous steady state (1.5) remains stable. Onset of instability occurs at $L = L_{\min}$ and for $L \geqslant nL_{\min}$ with n an integer greater than unity, other unstable modes will appear. This is illustrated in Figure 3 for a few values of B. This type of analysis has been developed in detail by

Hanson (1974) (see also Nitzan, Ortoleva and Ross, 1974). The conclusions are similar to those presented above where L is treated as a given parameter in the same way as A, D_X and D_Y. This approach is particularly of interest in the study of biological problems related, for example, to development and morphogenesis (Martinez, 1972; Babloyantz and Hiernaux, 1974).

2. Nonlinear Analysis: Methods

From the linear stability analysis one can infer the evolution beyond the critical point given by (2.10) to new steady state solutions of (1.2).

In the following sections we construct the analytical form of the steady state solution bifurcating beyond instability for the case of zero flux boundary conditions and summarize the results obtained by Auchmuty and Nicolis (1975) for fixed boundary conditions. We also report the behavior of the system in the unstable region as obtained by numerical integration of the nonlinear equations (1.2) on digital computer. The properties of these dissipative structures are analyzed and the theoretical results are compared with those of computer simulations.

Before presenting the explicit form of the new steady state solutions we first briefly recall the general features of the analytical method that will be used. Further details and justifications can be found in the paper by Auchmuty and Nicolis (1975). We also give some details about the numerical technique.

2.1. General Bifurcation Scheme. From the linear stability analysis of our model it follows that the linear differential-matrix operator $\mathscr{L}$ admits eigenfunctions corresponding to simple zero eigenvalues. In fact a bifurcation scheme could provide approximate steady state solutions in the neighborhood of any point on the marginal stability curve $B_{2c}(n)$ corresponding to such a null eigenfunction. But we will particularly consider the first bifurcation point arising for $n = n_c$ and $B_c = B_{2c}(n_c)$.

Inserting decomposition (2.1) into the rate equations (1.2) at the steady state, keeping this time the nonlinear contributions in x and y, we obtain:

$$\mathscr{L}_c \begin{pmatrix} x \\ y \end{pmatrix} = \begin{pmatrix} -h(x, y) \\ +h(x, y) \end{pmatrix} \tag{2.18}$$

where $\mathscr{L}_c$ is the linear operator (2.4) evaluated at the critical point (2.13) and

$$h(x, y) = (B - B_c)x + 2Axy + (B/A)x^2 + x^2y. \tag{2.19}$$

Again, the appropriate boundary conditions are given by (2.3). Vector $\begin{pmatrix} x \\ y \end{pmatrix}$

will be a solution of (2.18) provided $\mathscr{L}_c$ satisfies the solvability condition given by the Fredholm alternative:

$$\left\langle (x^+, y^+), \begin{pmatrix} -h \\ +h \end{pmatrix} \right\rangle = \int_0^L \mathrm{d}r(y^+ - x^+)h(x, y) = 0 \tag{2.20}$$

where (x^+, y^+) is the eigenfunction corresponding to a null eigenvalue of the adjoint of $\mathscr{L}_c$. From (2.4) one sees that both $\mathscr{L}_c$ and its adjoint have the same critical wave number n_c. The amplitudes of x^+ and y^+ will be different. This can be demonstrated by a relation similar to (2.16) for the amplitudes c_1 and c_2 of x^* and y^*.

In order to calculate explicitly the bifurcating solution one writes in the neighborhood of the critical point:

$$\begin{pmatrix} x \\ y \end{pmatrix} = \varepsilon \begin{pmatrix} x_0 \\ y_0 \end{pmatrix} + \varepsilon^2 \begin{pmatrix} x_1 \\ y_1 \end{pmatrix} + \varepsilon^3 \begin{pmatrix} x_2 \\ y_2 \end{pmatrix} + \cdots \tag{2.21}$$

$$B - B_c = \gamma = \varepsilon\gamma_1 + \varepsilon^2\gamma_2 + \cdots. \tag{2.22}$$

Introducing these expansions into (2.18), one gets upon identifying terms with equal powers of ε, the system of equations

$$\mathscr{L}_c \begin{pmatrix} x_k \\ y_k \end{pmatrix} = \begin{pmatrix} -a_k \\ a_k \end{pmatrix}, \quad 0 \leqslant k < \infty \tag{2.23}$$

supplied by the corresponding boundary conditions.

In these equations $a_k(r)$ involves the parameters of the kinetic equations, γ_j $(j = 1, 2, 3\ldots)$, $x_i(r)$ and $y_i(r)$ for $0 \leqslant i \leqslant k - 1$. The first expressions for a_k are

$$a_0(r) = 0 \tag{2.24}$$

$$a_1(r) = \gamma_2 x_0 + \frac{B_c}{A} x_0^2 + 2Ax_0y_0 \tag{2.25}$$

$$a_2(r) = \gamma_2 x_0 + \left(\gamma_1 + \frac{2B_c}{A} \cdot x_0 + 2Ay_0\right)x_1 + 2Ax_0y_1 + \frac{\gamma_1}{A} \cdot x_0^2 + x_0^2y_0. \tag{2.26}$$

From (2.24) it follows immediately that $\begin{pmatrix} x_0 \\ y_0 \end{pmatrix}$ are given by either (2.14) or (2.15) depending on the boundary conditions that are considered.

The validity of the solvability condition (2.20) to each order, i.e. for each function $a_k(r)$, leads to the determination of the coefficients γ_j and permits to express ε in terms of $(B - B_c)$ from (2.22). The explicit form of the bifurcating solution is then obtained by substituting ε as well as the solutions $\begin{pmatrix} x_i \\ y_i \end{pmatrix}$ of the successive approximations of (2.18) in (2.21).

2.2 Simulation Method. The following procedure has been adopted in the numerical computations:

(a) The linear range $0 \leqslant r \leqslant L$ is divided into a number $(M - 1)$ of equal space intervals Δr, defined by points 1 to M.

(b) At a given point i of this linear mesh, the spatial derivatives are approximated by central finite differences. Thus, e.g.

$$\left(\frac{\partial X}{\partial r}\right)_i = \frac{X_{i+1} - X_{i-1}}{2\Delta r}; \qquad \left(\frac{\partial^2 X}{\partial r^2}\right)_i = \frac{X_{i+1} - 2X_i + X_{i-1}}{(\Delta r)^2}.$$

(c) For each simulation the adopted boundary conditions are specified at points 1 and M:

the boundary concentrations are maintained symmetrically at their homogeneous steady state value: $X = A$, $Y = B/A$;

for null fluxes at the boundaries, the concentrations at points 1 and M evolve freely; the second spatial derivatives are approximated by:

$$\left(\frac{\partial^2 X}{\partial r^2}\right)_1 = \frac{2(X_2 - X_1)}{(\Delta r)^2}; \qquad \left(\frac{\partial^2 X}{\partial r^2}\right)_M = \frac{2(X_{M-1} - X_M)}{(\Delta r)^2}.$$

The initial condition consists in a slight modification of the homogeneous steady state (1.5) by applying a small perturbation to the concentration of X at one or more points of the linear array.

(d) In this way the partial differential equations (1.2) are replaced by a set of $2M$ ordinary differential equations which are integrated in time by means of a Runge–Kutta method with automatic step size regulation.

As regards the convergence of the numerical analysis, we note that for calculations performed with various numbers of space intervals ($M = 26, 51, 101$) the observed qualitative behavior is not altered. The quantitative differences become small as M increases.

Moreover, the convergence of the time integration was confirmed by using (for a few examples) other types of integration routines namely based on:

Hamming's predictor–corrector method initialized with Runge–Kutta;

Merson's fourth order method, which is a modified Runge–Kutta method with variable step length (Lange, 1960);

an extrapolation method consisting in an extension of Romberg integration (Burlish and Stoer, 1966).

A further check of the numerical results was provided by the use of the general

macroscopic evolution criterion $d_X P/dt \leqslant 0$ of Prigogine and Glansdorff (1971), in the particular suitable form proposed by M. Hanson (1974), i.e.

$$\frac{d_X P}{dt} = -R \int \sum_i (\dot{C}_i)^2 C_i^{-1} \, dr \leqslant 0$$

where C_i represents the concentrations of the different species, the equality sign referring to the time independent states. As both the concentrations themselves and their time rates of change are already required for the simulations, this inequality can easily be introduced as a test for the steady state results.

3. Zero Flux Boundary Conditions

3.1. Analytical Construction of the Solutions. In this section we apply the analytical method described in Section 2.1 to construct an approximate expression for the bifurcating dissipative structure in the case of zero flux boundary conditions. We have then:

$$\frac{d}{dr} x_k(0) = \frac{d}{dr} x_k(L) = \frac{d}{dr} y_k(0) = \frac{d}{dr} y_k(L) = 0 \quad (0 \leqslant k < \infty) \tag{2.27}$$

and the solvability condition (2.20) takes the explicit form:

$$\int_0^L a_k(r) \cos \frac{n_c \pi r}{L} \, dr = 0 \tag{2.28}$$

where we have taken into account that the amplitudes c_1^+ and c_2^+ can never be equal.

The procedure is now as follows:

(a) Introducing (2.25) in this compatibility condition for $k = 1$, one finds:

$$\gamma_1 = 0 \tag{2.29}$$

whether n_c odd or even.

(b) To take the calculations to the next order we need to determine the explicit form of $\begin{pmatrix} x_1 \\ y_1 \end{pmatrix}$. They are given by the solution of (2.23)–(2.27) with $k = 1$, i.e.:

$$\begin{aligned} D_X \cdot \frac{d^2 x_1}{dr^2} + (B_c - 1)x_1 + A^2 y_1 &= -a_1(r) \\ D_Y \cdot \frac{d^2 y_1}{dr^2} - B_c x_1 - A^2 y_1 &= +a_1(r) \end{aligned} \tag{2.30}$$

where

$$a_1(r) = \left\{ \frac{B_c}{A} c_1 + 2A c_2 \right\} c_1 \cos^2 \frac{n_c \pi r}{L}. \tag{2.31}$$

Solution for $x_1(r)$:

Adding these two equations one obtains

$$D_Y \cdot \frac{d^2 y_1}{dr^2} = -D_X \cdot \frac{d^2 x_1}{dr^2} + x_1. \tag{2.32}$$

Differentiating twice the first equation (2.30) leads after multiplying both sides by D_Y/A^2 and introducing (2.32), to a relation for x_1 only:

$$D_X D_Y \frac{d^4 x_1}{dr^4} + \{D_Y(B_c - 1) - A^2 D_X\} \frac{d^2 x_1}{dr^2} + A^2 x_1 = 2D_Y \beta \left\{ \frac{B_c}{A} c_1 + 2Ac_2 \right\} c_1 \cos \frac{2n_c \pi r}{L}. \tag{2.33}$$

To solve this equation we assume that x_1 has a fourier expansion

$$x_1 = \sum_{l=0}^{\infty} p_l \cos \frac{l\pi r}{L} \quad (l = \text{integer}). \tag{2.34}$$

Inserting (2.34) into (2.33) and using the orthogonality properties of $\cos(l\pi r/L)$ for different l's, we find

$$p_l = 0 \qquad \text{for } l \neq 2n_c$$

$$p_l = \frac{2D_Y \beta \alpha}{\Delta_l} \qquad \text{for } l = 2n_c$$

where

$$\alpha = \left(\frac{B_c}{A} c_1 + 2Ac_2 \right) c_1$$

$$\Delta_l = D_X D_Y \left(\frac{l\pi}{L} \right)^4 - [(B_c - 1)D_Y - D_X A^2] \left(\frac{l\pi}{L} \right)^2 + A^2.$$

Furthermore, $l = 0$ has to be rejected to be consistent with (2.13). One gets

$$x_1(r) = \frac{2D_Y \cdot \beta \alpha}{\Delta_l} \cos \frac{2n_c \pi r}{L}. \tag{2.35}$$

This expression can be simplified by noting that Δ_l is equivalent to the w-independent term Δ of the characteristic equation (2.6) and that we are concerned with simple zero eigenvalues. Δ_l may then be rewritten for $B = B_c$ as:

$$\Delta_l \simeq D_X D_Y \frac{\pi^4}{L^4} (l^2 - n_c^2)^2 = 9 D_X D_Y \beta^2. \tag{2.36}$$

This becomes an exact expression for $B_c = B_{\min}$ given by (2.12).

One finally obtains:

$$x_1(r) = \frac{2}{9} \cdot \frac{c_1^2}{AD_X\beta}\{2(D_X\beta + 1) - B_c\} \cos \frac{2n_c\pi r}{L}. \tag{2.37}$$

Solution for $y_1(r)$:

$y_1(r)$ can now be determined from the second equation (2.30) together with (2.32). This yields

$$y_1(r) = q_l \cos \frac{2n_c\pi r}{L} + q_0 \tag{2.38}$$

with

$$q_l = \frac{2}{9} \cdot \frac{c_1^2}{A^3 D_X\beta}[2(D_X\beta + 1) - B_c][\tfrac{7}{4}D_X\beta + 1 - B_c]$$

$$q_0 = -\frac{1}{2} \cdot \frac{c_1^2}{A^3}[2(D_X\beta + 1) - B_c]$$

(c) Using the expressions for (x_1, y_1) one may now determine γ_2 from (2.28) with $k = 2$. This can be written as:

$$\gamma_2 \int_0^L x_0 \cos \frac{n_c\pi r}{L}\, dr = \int_0^L dr\left\{-2\frac{B_c}{A} \cdot x_0x_1 - x_0^2y_0 - 2A(x_0y_1 + y_0x_1)\right\} \cos \frac{n_c\pi r}{L}.$$

Substituting (2.15), (2.37) and (2.38) in this equation one obtains:

$$\begin{aligned} \frac{\gamma_2}{c_1^2} &= -\frac{3}{4} \cdot \frac{D_X\beta + 1 - B_c}{A^2} + \frac{1}{A^2}[2(D_X\beta + 1) - B_c] \\ &\quad -\frac{2}{9} \cdot \frac{[2(D_X\beta + 1) - B_c][\frac{11}{4}D_X\beta + 2 - B_c]}{A^2 D_X\beta} \\ &= \phi(n_c, A, D_X, B_c). \end{aligned} \tag{2.39}$$

When n_c and B_c are given by (2.11)–(2.12) one gets instead

$$\begin{aligned} \frac{\gamma_2}{c_1^2} &= \frac{3}{4A}\left(\frac{D_X}{D_Y}\right)^{1/2}\left(1 + A\left(\frac{D_X}{D_Y}\right)^{1/2}\right) + \frac{1}{A^2}\left(1 - A^2\frac{D_X}{D_Y}\right) \\ &\quad - \frac{2}{9A^2}\left(\frac{D_Y}{D_X}\right)^{1/2}\left(1 - A^2\frac{D_X}{D_Y}\right)\left[\frac{1}{A} - A \cdot \frac{D_X}{D_Y} + \frac{3}{4} \cdot \left(\frac{D_X}{D_Y}\right)^{1/2}\right] \\ &= f(A, D_X/D_Y). \end{aligned} \tag{2.40}$$

These expressions can be positive, negative or zero depending on the values of

the involved parameters. If $\gamma_2 = 0$ the calculations should be continued to the next order, but this will seldom be the case. (2.39) or (2.40) may now be substituted in relation (2.22):

$$B - B_c = \gamma = \varepsilon^2\gamma_2 + \cdots.$$

Near $B = B_c$ one has then

$$\varepsilon = \pm\left(\frac{B - B_c}{\gamma_2}\right)^{1/2} \quad \text{for } \gamma_2 > 0,\ B > B_c$$

or

$$\varepsilon = \pm\left(\frac{B_c - B}{\gamma_2}\right)^{1/2} \quad \text{for } \gamma_2 < 0,\ B < B_c.$$

The bifurcating non uniform steady state solution near $B = B_c$ is thus approximated by

$$\begin{aligned} x(r) &= \pm\left(\frac{B - B_c}{\phi}\right)^{1/2} \cos\frac{n_c\pi r}{L} \\ &\quad + \frac{2}{9}\cdot\frac{B - B_c}{\phi}\cdot\frac{2(\beta D_X + 1) - B_c}{AD_X\beta}\cos\frac{2n_c\pi r}{L} \\ y(r) &= \pm\left(\frac{B - B_c}{\phi}\right)^{1/2}\cdot\frac{D_X\beta + 1 - B_c}{A^2}\cdot\cos\frac{n_c\pi r}{L} \\ &\quad + \frac{2}{9}\cdot\frac{B - B_c}{\phi}\cdot\frac{[2(\beta D_X + 1) - B_c][\frac{7}{4}D_X\beta + 1 - B_c]}{A^3D_X\beta}\cos\frac{2n_c\pi r}{L} \\ &\quad - \frac{1}{2}\cdot\frac{B - B_c}{\phi}\cdot\frac{2(\beta D_X + 1) - B_c}{A^3}. \end{aligned} \tag{2.41}$$

When $\gamma_2 > 0$ (2.41) holds for $B > B_c$ while for $\gamma_2 < 0$ it applies to $B < B_c$. This, together with the theorems about uniqueness and boundedness of the solutions of (1.2) for small positive B presented by Nicolis and Auchmuty (1974) (which may be readily extended to zero flux boundary conditions), suggest the following bifurcation diagrams:

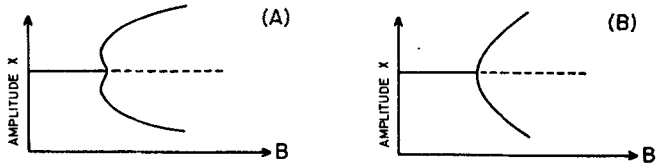

Figure 4. Bifurcation diagrams for n_c odd or even.
(A): $\gamma_2 < 0$; (B): $\gamma_2 > 0$.

We will comment on these diagrams and related properties in the next section.

3.2. Properties of the Dissipative Structures. We now investigate the properties of the spatial organization emerging beyond instability and compare the theoretical predictions with the results of computer simulation.

A. General behavior. In order to compare the theoretical and simulation

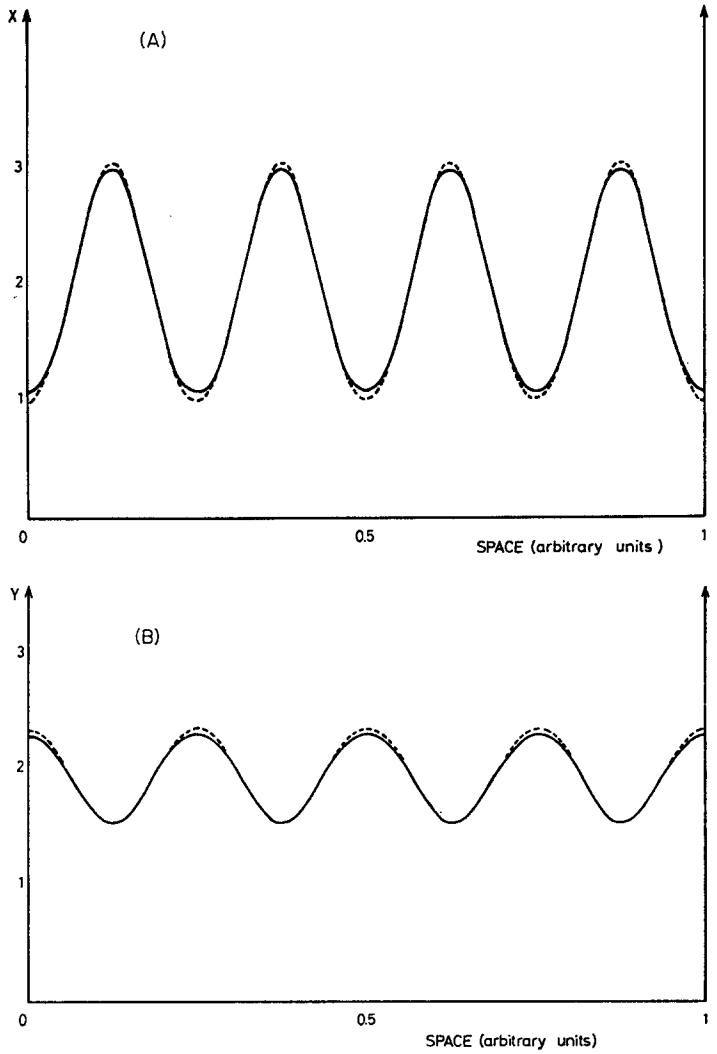

Figure 5. Steady state dissipative structure for zero flux boundary conditions. Dashed lines: analytical curves given by (2.41): solid lines: result of the numerical integration of (1.2) on digital computer. The curves have been established for $A = 2$, $L = 1$, $B = 4$, $D_X = 1.6 \times 10^{-3}$, $D_Y = 8.0 \times 10^{-3}$. The critical wave number is $n_c = 8$ and $B_c = 3.602$

approaches we introduce the numerical values used for stability diagram (B) in Figure 1 into expression (2.39). This leads to a positive value of ϕ and corresponds therefore to the bifurcation type described in Figure 4A. Figure 5 shows the non uniform concentration profiles of the intermediate species X and Y as obtained both by numerical integration of (1.2) and calculation of (2.41), for $B = 4$. The curves are in very good agreement: the small discrepancies must be attributed to the extension of the theoretical relations for values of B which are no longer in the direct neighborhood of the critical point. The correspondence between the two methods indeed improves considerably when B tends to B_c, but the amplitude of the dissipative structure then becomes very small. This shows that (2.41) represents a good approximation for the spatial organization even at greater distance of the instability point.

Furthermore one sees that the shape of the first bifurcating dissipative structure is strongly influenced by the form of the critical mode: the new profiles have a number of well defined minima and maxima corresponding to n_c. This is confirmed by a great number of calculations corresponding to various values of the critical wavenumber.

B. Properties. A closer inspection of the space organization shows the following properties:

(a) *spatial regularity.* (2.41) contains only two terms: the critical mode and a first harmonic. This simple form is essentially related to the boundary conditions. The harmonic term introduces only a slight distortion of the monochromatic wave form of the critical mode and does not alter significantly the spatial regularity of the solutions. This agrees with the results of numerical integration which leads to almost entirely regular concentration profiles (Figures 5–8).

(b) *influence of the symmetry of the critical mode.* The theoretical expressions are qualitatively the same whether n_c is even or odd. However as the dominant contribution is proportional to $\cos(n_c\pi r/L)$, (2.41) implies the appearance of a macroscopic gradient along the system each time n_c is an odd number: the values of the concentrations are then different at the two boundaries $r = 0$ and $r = L$. As shown in Figure 6, computer simulation confirms the possibility of spontaneous onset of polarity in a previously homogeneous system subjected to zero flux boundary conditions.

(c) *degeneracy of solutions.* The solutions (2.41) introduce a critical exponent of $\frac{1}{2}$ and are thus degenerate: at the critical point the system exhibits a symmetry-breaking transition to two new possible steady states. The particular

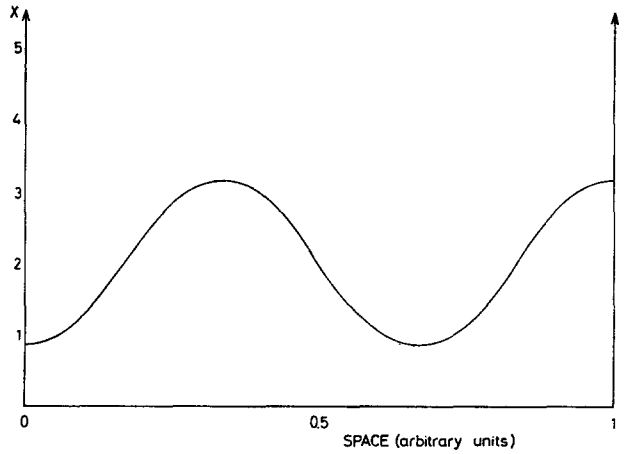

Figure 6. Polar dissipative structure in the case of an odd critical wave number. Numerical values used: $A = 2$, $L = 1$, $B = 4.9$, $D_X = 10^{-2}$, $D_Y = 3.6 \times 10^{-2}$; $n_c = 3$ and $B_c = 4.25$

form which will appear depends on the initial conditions. This is entirely confirmed by the numerical results. Let us apply a single, isolated perturbation to the homogeneous steady state as initial condition. Depending on the sign and location of the perturbation one observes two different solutions. Figure 7 presents a typical example of these degenerate states which are opposite to each other.

(d) *multiplicity of solutions.* Computer simulations have shown that more than one couple of degenerate structures, each corresponding to different wavelength and amplitude, can appear simultaneously. This occurs under the following conditions:

— the values of B are large;
— the system is submitted to different simultaneous initial perturbations;
— the location of those multiple perturbations obey certain rules.

This situation is illustrated in Figure 8. For the same values of the parameters as used in Figure 7, one observes three different stable dissipative structures (with respectively 8, 9 or 10 extrema) depending on the initial conditions. As before each new structure has its 'symmetrical'.

This phenomenon could be understood on the basis of equations (2.41) which could in fact provide approximations for the birfurcating steady state solutions not only in the neighborhood of the critical point given by (2.13) but also in the neighborhood of any solution of the marginal stability relation (2.10). In principle each time B is crossing a point on the marginal stability curve cor-

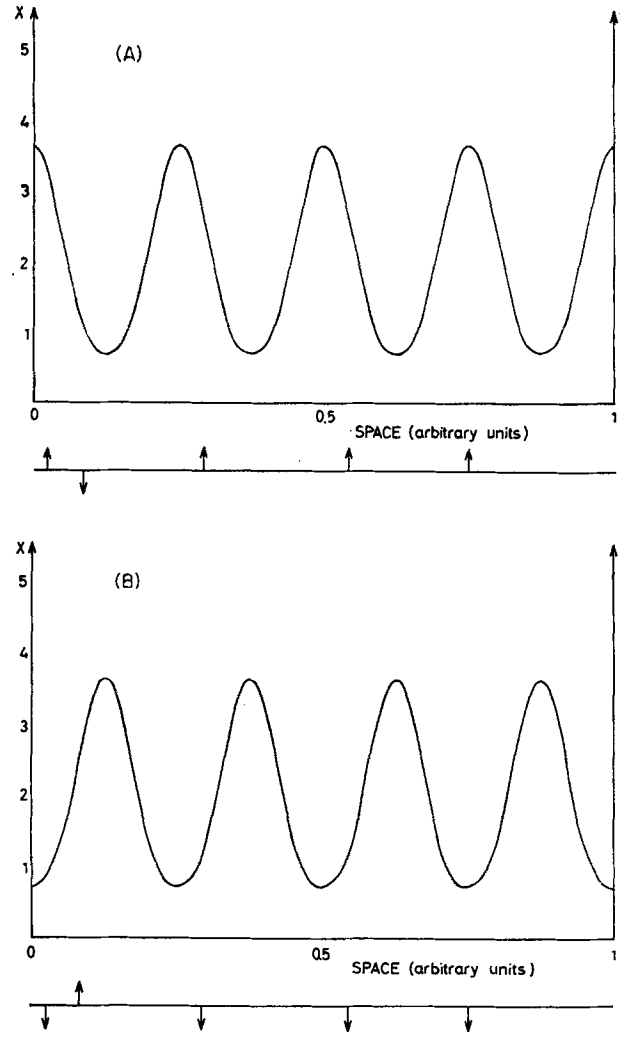

Figure 7. Degenerate steady state dissipative structures obtained for the same values of the parameters, by a single initial perturbation of the homogeneous steady state (1.4) of the same strength but opposite sign (zero flux boundary conditions). The arrows show for some points the sign of the perturbation leading to the corresponding spatial distribution. $B = 4.6$ and all the other parameters have the same value as in Figure 5

responding to a null eigenfunction of the linear operator $\mathscr{L}$, a new solution of the steady state equations (2.18) could appear and in this way an infinite number of solutions should exist. But the stability of the successive bifurcating solutions cannot be guaranteed *a priori* in the framework of a perturbation analysis.

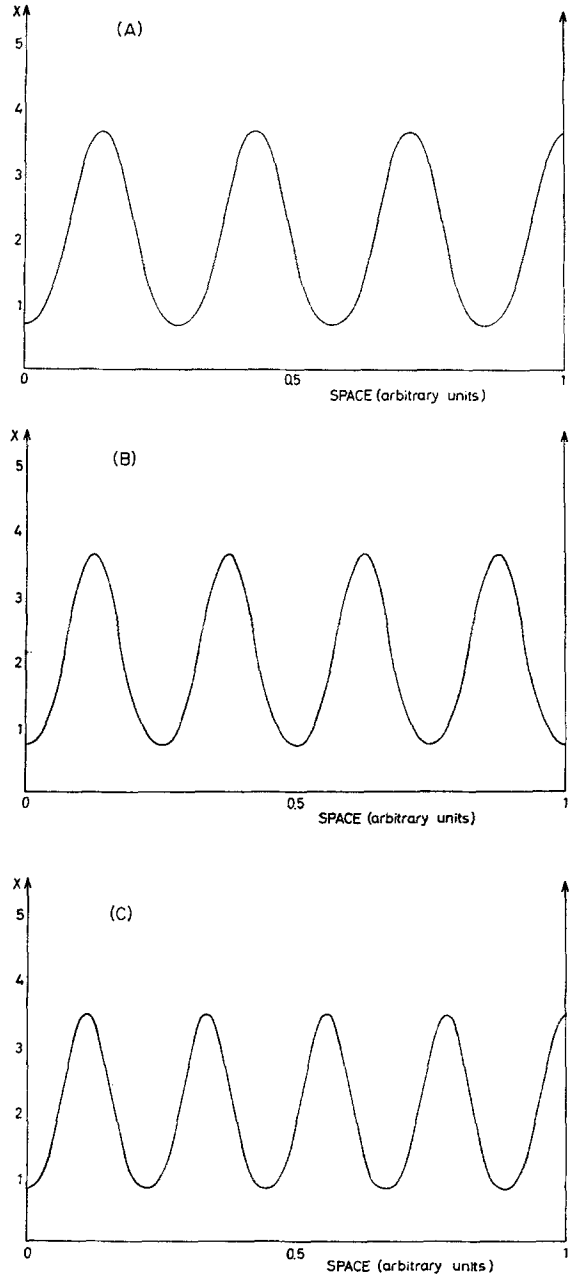

Figure 8. Steady state profiles obtained for the same values of the parameters but different initial conditions. For instance, one obtains the spatial distributions with 8, 9 or 10 extrema shown here above when a positive perturbation applied at point 9 is combined with a second perturbation of same sign and strength respectively at points: 21, 48 or 72; 17, 34, 43; 55 or 70. The numerical values of the parameters are the same as in Figure 7.

Various computer simulations for $B \gg B_c$ indicate that there is a *finite multiplicity* of stable solutions corresponding to the fastest growing unstable modes according to the linear stability analysis. This can be seen explicitly on Figure 2 where $n = 7$, $n = 8$ and $n = 9$ appear as the leading modes for the numerical values corresponding to our previous example (Figure 8). The existence of unstable modes whose amplification factors are of the same order of magnitude as that of the critical one is due to the fact that the successive instabilities appear for very close values of B.*

(e) *amplitude.* The amplitude of the dissipative structures arising by computer simulation appears to be concave in the quantity $(B - B_c)$, where B_c is the value of B on the neutral stability curve, in qualitative agreement with the theoretical predictions.

(f) *mean values.* The total amount of constituent X in the system is conserved during the symmetry-breaking transition to the dissipative structure. Indeed evaluation of

$$\bar{x} = \frac{1}{L}\int_0^L x(r)\,\mathrm{d}r \quad \text{and} \quad \bar{y} = \frac{1}{L}\int_0^L y(r)\,\mathrm{d}r$$

leads to:

$$\bar{x} = 0 \tag{2.42}$$

$$\bar{y} = -\frac{B - B_c}{\gamma_2} \cdot q_0. \tag{2.43}$$

$\bar{x}$ is thus invariant. This is a direct consequence of the boundary conditions and does not depend on the degree of approximation. Indeed adding the two equations (1.2) at the steady state one obtains:

$$X = A + D_X \frac{\mathrm{d}^2 X}{\mathrm{d}r^2} + D_Y \cdot \frac{\mathrm{d}^2 Y}{\mathrm{d}r^2}$$

and the mean value of X in the interval $(0, L)$ with the boundary conditions (1.3) is given by:

$$\bar{X} = A + \frac{1}{L}\left\{D_X \frac{\mathrm{d}X}{\mathrm{d}r} + D_Y \cdot \frac{\mathrm{d}Y}{\mathrm{d}r}\right\}_0^L = A.$$

Since the non zero contribution to $\bar{y}$ comes from a small term proportional to $(B - B_c)$ and does not depend on the dominant term proportional to $(B - B_c)^{1/2}$, $\bar{y}$ can be considered as an approximate invariant.

* Recent simulations suggest that the evolution to a spatial dissipative structure depends on the boundary condition as well as on the type of the initial perturbation. In particular, non-isolated perturbations extending throughout the reaction space can be attracted to a solution other than the first bifurcating ones.

(g) *entropy production.* The entropy production of the system is also unaffected by the transition at the bifurcation point. To see this we introduce small inverse reaction rates in the reaction scheme (1.1). The total entropy production is then given by:

$$P = \int_0^L \mathrm{d}r\Big\{(A - kX)\ln\frac{A}{kX} + (BX - kYD)\ln\frac{BX}{kYD} + (X^2Y - kX^3)\ln\frac{Y}{kX} + (X - kE)\ln\frac{X}{kE} + \frac{D_X}{X}\cdot\left(\frac{\partial X}{\partial r}\right)^2 + \frac{D_Y}{Y}\cdot\left(\frac{\partial Y}{\partial r}\right)^2\Big\}.$$

Upon keeping terms of $\theta(1)$ and $\theta(\ln k)$ but not of order $\theta(k)$ one gets, with the relation $X = A + x$:

$$P = \int_0^L \mathrm{d}r\Big\{A\ln A + (A + x)B\ln\frac{B}{D} - (A + x)\ln E\Big\} + D_X\Big[\ln X\frac{\partial X}{\partial r}\Big]_0^L + D_Y\Big[\ln Y\cdot\frac{\partial Y}{\partial r}\Big]_0^L - (2B + 1)\ln k(A + \bar{x}) + D_X\ln k\Big[\frac{\partial X}{\partial r}\Big]_0^L.$$

Using (2.42) and comparing with the entropy production at the uniform steady state one gets:

$$\Delta P = 0.$$

If, on the other hand, one compares the entropy production per unit mass, between the homogeneous steady state and the dissipative structure:

$$\Delta\left(\frac{P}{M}\right) = \frac{P_0 + \Delta P}{M_0 + \Delta M} - \frac{P_0}{M_0} = -P_0\cdot\frac{\Delta M}{(M_0 + \Delta M)M_0} \simeq -P_0\cdot\frac{\Delta M}{M_0^2} \quad \text{(for small } \Delta M\text{)}$$

one finds:

$$\Delta\left(\frac{P}{M}\right) \simeq 2\ln k(1 + B_c)\frac{A^3}{(A^2 + B_c)^2}\cdot\bar{y} \neq 0$$

which can be positive or negative depending on the sign of $\bar{y}$ as given by (2.43).

4. Fixed Boundary Conditions

4.1. Summary of Analytical Results. In order to establish a comparison with the numerical data of computer simulation we briefly resume the theoretical

results obtained by Auchmuty and Nicolis (1974) for fixed boundary conditions. In this case:

$$x_k(0) = x_k(L) = y_k(0) = y_k(L) = 0 \quad (0 \leqslant k < \infty) \tag{2.44}$$

and the solvability condition (2.20) has the form:

$$\int_0^L \mathrm{d}r \cdot a_k(r) \sin \frac{n_c \pi r}{L} = 0. \tag{2.45}$$

In contrast with the case of zero flux boundary conditions the behavior of the solutions depends now crucially on the symmetry properties of the critical mode. For B near B_c, one finds when:

(a) n_c *is even*:

$$x(r) = \pm \left(\frac{B - B_c}{\phi}\right)^{1/2} \sin \frac{n_c \pi r}{L} - \frac{B - B_c}{\phi} \cdot \frac{8\beta}{\pi^5 D_X A} \times [2(D_X\beta + 1) - B_c] \sum_{l\,\mathrm{odd}}^{\infty} \frac{l}{(l^2 - n_c^2)^2(l^2 - 4n_c^2)} \cdot \sin \frac{l\pi r}{L} \tag{2.46}$$

where ϕ again is an expression containing A, D_X, B_c and n_c which can be either positive or negative. There is a similar expression for $y(r)$. The corresponding bifurcation diagrams are of the same type as those depicted on Figure 4.

(2.46) shows following properties:

(1) The solutions are degenerate due to the critical exponent $\frac{1}{2}$ in the dominant approximation. The system exhibits therefore a symmetry-breaking transition to two possible new steady states.

(2) The infinite series appearing in (2.46) introduces subharmonical terms which constitute a source of spatial asymmetry. This is a direct consequence of the boundary conditions and has to be contrasted with the results obtained in Section 3.1. The dominant contribution to the distortion is given by the term whose l is the odd number closest to n_c or $2n_c$. It is interesting to note that for $B_c = 2(D_X\beta + 1)$ this infinite series cancels.

(3) The total amount of X and Y in the system is not conserved during the transition to the dissipative structures. The entropy production is also affected.

(b) n_c *is odd*:

In the dominant approximation ε, one obtains:

$$x(r) = -\tfrac{3}{8}(B - B_c) \cdot \frac{n_c \pi}{L} \cdot A[2(D_X\beta + 1) - B_c]^{-1} \sin \frac{n_c \pi r}{L} + \theta[(B - B_c)^2] \tag{2.47}$$

with a similar expression for $y(r)$.

In contrast with the other cases (2.41) and (2.46), this new branch of the solution is defined for B both above and below B_c. Since one can show that there is a unique non negative solution $X(r)$ when B is small and positive, and that $X(r)$ possesses an *a priori* bound, the bifurcation diagram for this case can be depicted as follows:

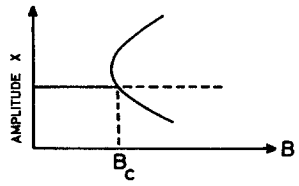

Figure 9. Bifurcation diagram for n_c odd (fixed boundary conditions)

Thus:

(1) the bifurcation is not accompanied by symmetry breaking as there exists only one branch crossing the critical point;

(2) (2.47) shows the possibility of an hysteresis effect:

for $B < B_c$, two new solutions may appear; there are thus three solutions: the thermodynamic branch and two dissipative structures, one of which, at least, is unstable;

for $B \geqslant B_c$, there may be two dissipative structures one of which requires an abrupt transition from the homogeneous steady state.

for B sufficiently large, these two dissipative structures will again be reached by perturbing slightly the uniform solution and the property of symmetry breaking is thus restored.

4.2. Properties of the Dissipative Structures

4.2.1. n_c even

A. General behavior. The numerical values corresponding to $A = 2$, $L = 1$, $D_X = 1.6 \times 10^{-3}$, $D_Y = 6.0 \times 10^{-3}$ lead to a positive value of ϕ which permits us to calculate the form of $x(r)$ and $y(r)$ given by (2.46) for $B > B_c$. The steady state solutions obtained in this way, on retaining the first 15 terms of the odd series are shown on Figures 10 and 11, and compared with those obtained by numerical integration of (1.2) on computer.

(a) B near B_c (Figure 10): The two approaches agree very well. Both predominant influence of the critical mode and its distortion are clearly seen.

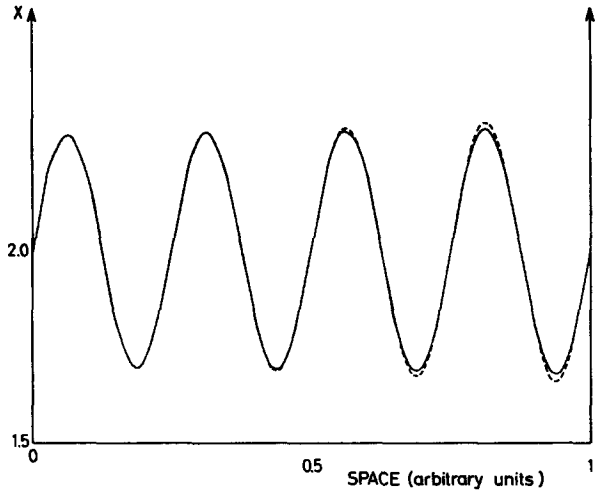

Figure 10. Steady state dissipative structure for fixed boundary conditions and $B \simeq B_c$. Dashed line: analytical curve given by (2.46); solid line: result of the numerical integration of (1.2) on digital computer. The following numerical values of the parameters have been chosen: $A = 2$, $L = 1$, $D_X = 1.6 \times 10^{-3}$, $D_Y = 6.0 \times 10^{-3}$, $B = 4.17$. The critical wave number is $n_c = 8$ and $B_c = 4.133$. The boundary values for X and Y are: $X = A = 2$, $Y = B/A = 2.085$

One observes that distortion acts to enhance the successive maxima (and diminish the successive minima) from the boundary at $r = 0$ to the boundary at $r = L$. Moreover one notes that the dominant contributions to this distortion are indeed given by the predicted terms of the infinite series, for our example: $\sin(7\pi r/L)$ and $\sin(9\pi r/L)$.

(b) $B > B_c$ (Figure 11): Comparison between theoretical and computer simulation results shows that the agreement becomes very poor when the calculations are performed for values of B which do not correspond to the *direct* neighborhood of B_c. Indeed direct numerical integration of (1.2) indicates that the influence of the critical wave form continues to prevail in determining the number of extrema of the final steady state but the spatial asymmetry is now entirely different than for $B \simeq B_c$: near the boundaries the maxima are enhanced and minima diminished. A great number of calculations with various initial conditions have shown that this type of asymmetry does not depend on the location of the initial perturbation. Hence expression (2.46) no longer applies as it is for larger values of B.

These results could be explained by an instability of the first bifurcating branch beyond a certain distance from B_c and the occurrence of a *secondary*

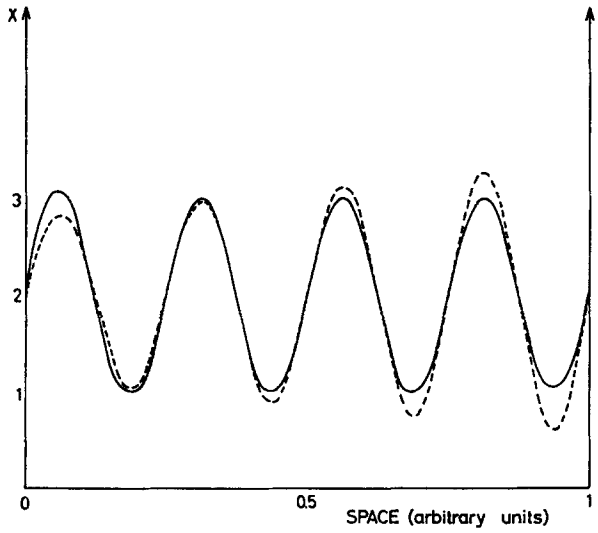

Figure 11. Steady state dissipative structure for fixed boundary conditions and $B > B_c$. Dashed line: analytical curve given by (2.46); solid line: result of the numerical integration of (1.2) on digital computer. $B = 4.6$; other parameters are as in Figure 10. The boundary values for X and Y are: $X = A = 2$, $Y = B/A = 2.3$

bifurcation may be responsible for the change in behavior of the solution observed numerically.

On the other hand, for the values of parameters we considered the spacing between the values of B corresponding to the first successive unstable modes emerging from the thermodynamic branch ($n = 8$ and $n = 9$) is small: $\Delta B = B_c(n = 9) - B_c(n = 8) = 0.0469$. One observes that the change in behavior of the solution appears near the critical value of the next (odd) mode. There could thus exist a relation between the appearance of the new unstable mode and the change in behavior of the first bifurcating solution.

This is supported by the further computer simulations: the spatial asymmetry subsists even for $B_c = 2(\beta D_X + 1)$. Since in this case the infinite series in (2.46) disappears, the observed distortion must be related either to a non negligible influence of the neglected higher order terms or more probably to the occurrence of a secondary bifurcation.

One should compare these results with those of the zero flux boundary conditions where the distance from B_c and the quasi-simultaneously unstable modes had apparently a smaller influence on the final shape of the steady state.

B. Particular properties

(a) *Degeneracy of solutions:* Since the theoretical prediction of degeneracy is related to the dominant contribution proportional to the critical mode, this property could extend to higher values of B. This is indeed confirmed by the computer simulations. Figure 12 represents two degenerate solutions obtained for $B \gg B_c$. They are enantiomorphs. The system tends to one or the other depending on the initial perturbation.

(b) *Multiplicity of solutions:* Multiplicity of solutions for $B \gg B_c$ appears as for zero flux boundary conditions: upon mixing the initial perturbations one obtains again a finite number of stable solutions corresponding to the fastest growing modes of the linear stability analysis. A characteristic example is shown in Figure 13.

(c) *Spatial asymmetry:* The spatial asymmetry at the boundaries described above becomes more pronounced when one enters more deeply into the unstable region as shown in Table I. However, the maximum observed amplitude is in good agreement with the theorem of boundedness demonstrated by Auchmuty and Nicolis (1974), i.e.:

$$X(r) \leqslant A + \frac{D_Y}{D_X} \cdot \frac{B}{A}$$

$$Y(r) \leqslant \frac{B}{A} + \frac{D_X}{D_Y} \cdot A$$

which is also indicated in Table I.

TABLE I

D_Y	B	Δ^*	Calculated upper bound		Maximum observed amplitudes	
			X	Y	X	Y
	4.0	1.09	12.0	2.4	3.322	2.349
0.0080	4.2	1.14	12.5	2.5	3.722	2.489
	4.6	1.34	13.5	2.7	4.476	2.716
	4.3	1.002	10.006	2.683	2.644	2.489
0.0060	4.6	1.031	10.625	2.833	3.126	2.817
	5.0	1.085	11.375	3.033	3.674	3.118

* Δ = max 1/max 2, i.e.: the ratio of the amplitudes of the first (highest) and second maximum. *Numerical values of the other parameters:* $A = 2$, $L = 1$, $D_X = 1.6 \times 10^{-3}$.

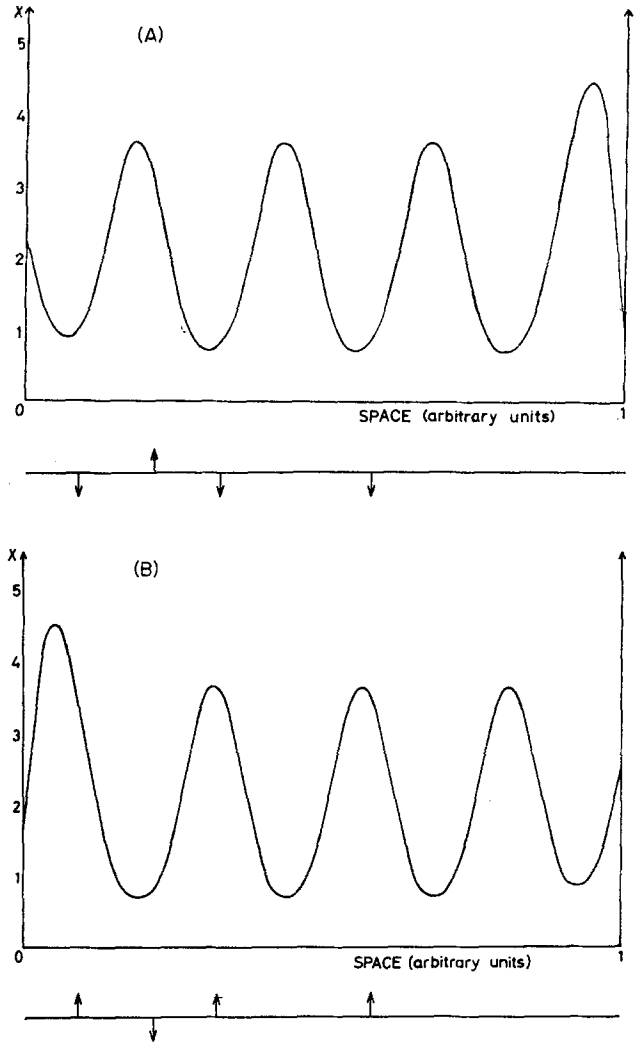

Figure 12. Degenerate steady state dissipative structures obtained for the same values of the parameters, by a single initial perturbation of the homogeneous steady state (1.5) of the same strength but opposite sign (fixed boundary conditions). The arrows show for some points the sign of the perturbation leading to the corresponding spatial structure. Numerical values used: $A = 2$, $L = 1$, $D_X = 1.6 \times 10^{-3}$, $D_Y = 8.0 \times 10^{-3}$, $B = 4.6$. The homogeneous steady state concentrations $X = A$, $Y = B/A$ are maintained at the boundaries

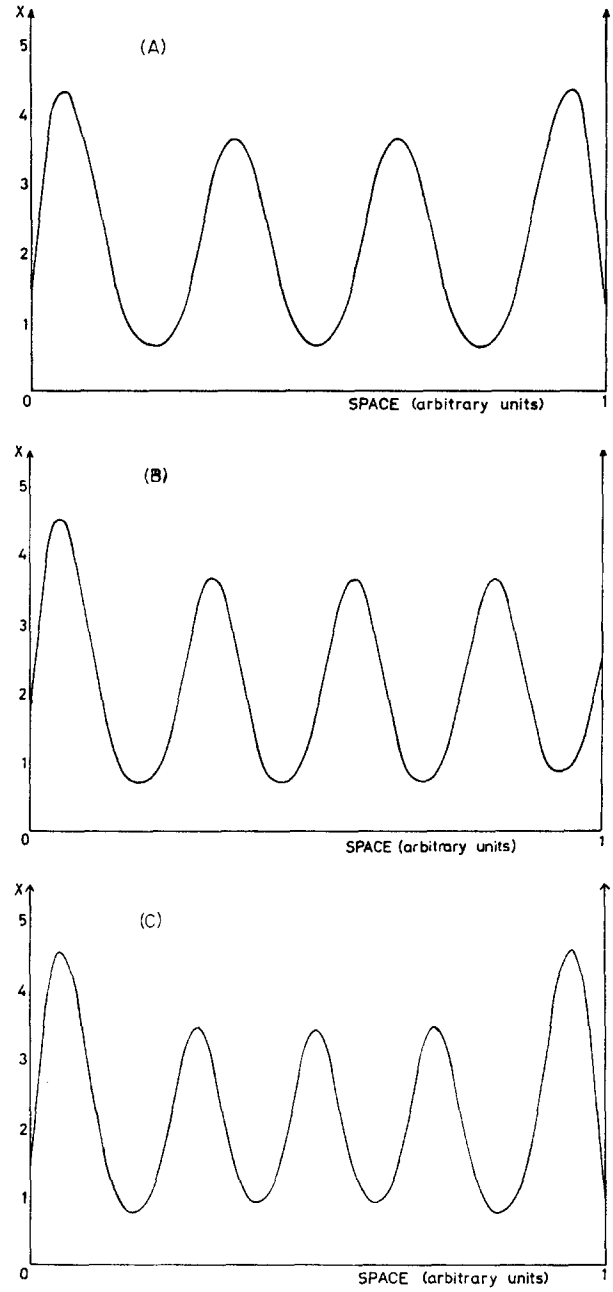

Figure 13. Steady state profiles obtained for the same values of the parameters but different initial conditions. For instance, one obtains the spatial structures with 7, 8 or 9 extrema shown here above when a positive perturbation at point 9 is combined with a second perturbation of the same strength and sign respectively at points: 17, 20 or 43; 30, 55, 81; 23, 50. The numerical values of the various parameters are the same as in Figure 12

4.2.2. n_c odd

A detailed investigation of (2.47) has not been performed. However, numerical integration of (1.2) leads to the following observations:

(1) for $B \gg B_c$, both degeneracy and finite multiplicity of solutions appear in the same way as described in the preceeding sections. The solutions show the same characteristic spatial asymmetry as for n_c even.

(2) for $B \geqslant B_c$, two stable degenerate solutions appear. They have small amplitudes and their overall shape is dominated by the critical wave form.

(3) for $B \leqslant B_c$, a transient non uniform state appears: upon a finite amplitude perturbation of the homogeneous steady state, the system first evolves toward a structured state with a number of extrema corresponding to n_c; but the system homogenizes slowly returning to the thermodynamic branch. Our computer simulations leave the question of stability of those subcritical branches still open.

These results support the general features of the bifurcation diagram depicted on Figure 9.

The existence of stable subcritical branches was also investigated, for $n_c = 1$ by this time using the length L as bifurcating parameter. Two stable 'symmetrical' subcritical branches were found for $L \leqslant L_c = 0.12566$ and $B = 3.6$ ($A = 2$, $D_X = 0.0016$, $D_Y = 0.0080$). They require a finite perturbation to be reached when $L \leqslant L_c$, small perturbations being sufficient for $L \geqslant L_c$.

5. Periodic Boundary Conditions

We also investigated numerically the case of a system subjected to periodic boundary conditions:

$$X(0) = X(L),\ Y(0) = Y(L) \quad (t \geqslant 0). \tag{2.48}$$

The perturbations to be considered for the linear stability analysis of the thermodynamic branch (1.5) now have the form:

$$\begin{pmatrix} x \\ y \end{pmatrix} = \begin{pmatrix} c_1 \\ c_2 \end{pmatrix} e^{w_n t} \cdot e^{\frac{2\pi i n r}{L}} \quad (n = 0, 1, 2 \ldots) \tag{2.49}$$

and relations (2.7)–(2.13), where β is now given by $\beta = (2\pi n/L)^2$, remain valid.

The numerical calculations were performed for the particular case of a closed ring divided into M equally spaced intervals. Then (2.48) becomes:

$$\begin{aligned} X_{M+1} &= X_1, \qquad X_0 = X_M \\ Y_{M+1} &= Y_1, \qquad Y_0 = Y_M. \end{aligned} \tag{2.50}$$

As previously, spatial non uniform solutions arise beyond instability. They

correspond to a regular periodicity in space. Insofar as the number of space intervals is large enough, the structures which are obtained for different initial conditions (i.e. sign, location and number of perturbations) are now superposable by translation and in the limit of a continuous space one should observe an infinity of solutions differing only by phase. A typical example is illustrated in Figure 14.

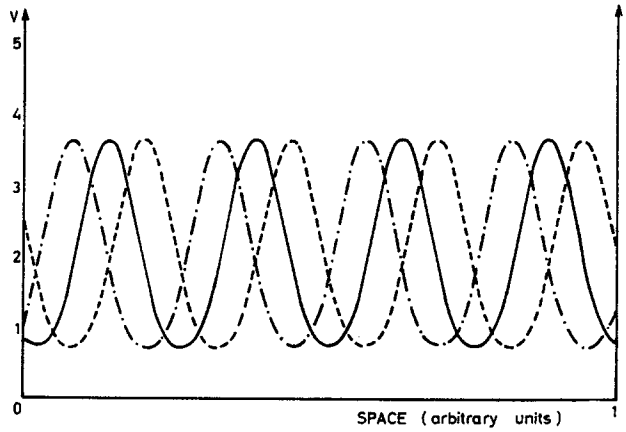

Figure 14. Stationary concentration profiles of X for periodic boundary conditions ($X_{M+1} = X_1$, $Y_{M+1} = Y_1$) and different initial conditions.

———: initial perturbations $\Delta X = +0.02$ at points 9 and 21.

– – – –: initial perturbation $\Delta X = +0.02$ at point 21

–·–·–·: initial perturbation $\Delta X = +0.02$ at point 9

Numerical values used: $A = 2$, $L = 1.01$, $B = 4.6$, $D_X = 1.6 \times 10^{-3}$, $D_Y = 8.0 \times 10^{-3}$ ($B_c = 3.598$ and $n_c = 4$)

6. Conclusion

The preceeding results give some insight into the mechanisms of spatial ordering in a previously homogeneous medium. They particularly underline the influence of boundary and initial conditions on the variety of spatial patterns which emerge beyond an instability.

The nature of the boundary conditions appear of great importance in performing the bifurcation analysis.

For fixed boundary conditions, the symmetry of the critical mode has to be taken into account: even and odd wave numbers have to be treated separately and lead to different types of solutions and bifurcation mechanisms; symmetry breaking is not necessarily involved.

For zero flux boundary conditions, however, both even and odd critical wave numbers lead to the same theoretical expressions and the new steady state

appears always through a symmetry-breaking transition. But even in this case, the symmetry of the critical mode plays a non negligible role for the shape of the bifurcating dissipative structure, as it may lead to the spontaneous appearance of an asymmetry in the boundary values of the concentrations.

Moreover, the boundary conditions influence strongly the form of the theoretical expressions. The complex relations including infinite series for Dirichlet conditions, are replaced by much simpler ones when impermeable boundaries apply. This is reflected in the spatial asymmetry (or symmetry) of the bifurcating solutions.

An interesting effect appears from computer simulations (which allow the study for greater B's), when the spacing of the values of B corresponding to successive unstable modes is small. Although the shape of the spatial pattern is still to a great extent dominated by the critical mode, distortion is influenced by the other leading unstable modes. The analytical expressions which were constructed are limited to a very small neighborhood of the critical point and theoretically the existence of secondary bifurcations remains to be analyzed for both fixed and zero flux boundary conditions. It is interesting to note that this point becomes even more important in the 2-dimensional analysis where, besides the fact that completely degenerate modes appear more frequently, the number of quasi-simultaneously unstable modes increases considerably, in particular for zero flux boundary conditions.

On the other hand theoretical and computer calculations show the fundamental importance of the initial conditions for the particular spatial pattern which appear beyond instability.

Both approaches indicate the possibility of degenerate steady state solutions. To which of those solutions the system tends asymptotically as $t \to \infty$ is determined by the initial state. In addition, computer simulations show that new couples of structures emerge when one enters more deeply in the unstable region. Those structures which appear after the first bifurcations remain stable even for higher values of B.

III. LOCALIZED STEADY STATE DISSIPATIVE STRUCTURES

1. Description and Properties

The spatial dissipative structures described in the preceeding chapter extend throughout the whole system: this is a consequence of assuming a uniform medium where initial and final products' concentrations are maintained constant in time and space.

In this section we discuss the case of unstable transitions when the condition of uniform medium is suppressed by allowing reactant A to diffuse and react

freely inside the system. We shall see that as a result of the spatial inhomogeneity of A the dissipative structures may now become localized inside natural boundaries within the reaction space.

We first present some numerical results obtained for non uniform medium. We then establish a comparison with the theoretical development reported in the paper by Auchmuty and Nicolis (1975).

As for the 'homogeneous' case we write the conservation equations for the intermediate species X and Y. They are now supplemented by an equation for the evolution of A.

Thus, according to reaction scheme (1.1):

$$\frac{\partial X}{\partial t} = A(r) + X^2Y - (B + 1)X + D_X \cdot \frac{\partial^2 X}{\partial r^2} \tag{3.1}$$

$$\frac{\partial Y}{\partial Y} = BX - X^2Y + D_Y \cdot \frac{\partial^2 Y}{\partial r^2}$$

and the additional equation:

$$\frac{\partial A}{\partial t} = -A + D_A \cdot \frac{\partial^2 A}{\partial r^2} \quad (0 \leqslant r \leqslant L). \tag{3.2}$$

The boundary conditions are:

$$\begin{aligned} X(0) &= X(L) = \bar{X} \\ Y(0) &= Y(L) = \bar{Y} \\ A(0) &= A(L) = \bar{A}. \end{aligned} \tag{3.3}$$

By setting $\bar{X} = \bar{A}$ and $\bar{Y} = B/\bar{A}$ we suppress spurious boundary layers.

The solution of (3.2)–(3.3) at the steady state is straightforward and gives:

$$A_0(r) = \bar{A} \cdot \frac{\cosh\left[2\alpha(r - L/2)\right]}{\cosh \alpha} \tag{3.4}$$

with $\alpha = (\frac{1}{4}D_A)^{1/2}$. System (3.1)–(3.3) has thus to be solved for X and Y only, A being a given function of r.

However, because of the spatial dependence of A, the mathematical treatment of the rate equations (3.1) becomes more difficult.

The steady state solutions $(X_0(r), Y_0(r))$ on the thermodynamic branch can no longer be determined exactly. Approximate steady state solutions, reducing to (1.5) in the homogeneous limit $D_A \to \infty$, have been obtained using the local potential variational technique. Figure 15 shows an example of these steady state concentration profiles for $D_A = 0.197$. Details of calculation are given in the references by Herschkowitz-Kaufman and Platten (1971) and

Herschkowitz-Kaufman (1973). We notice that their form is roughly given by an extension of the formulas (1.5) and is only slightly modified by diffusion.

Since the linear stability equations now have variable coefficients and the boundary value problem for the eigenfunctions is not self-adjoint, the stability problem is much more difficult. Consequently we again used the local potential

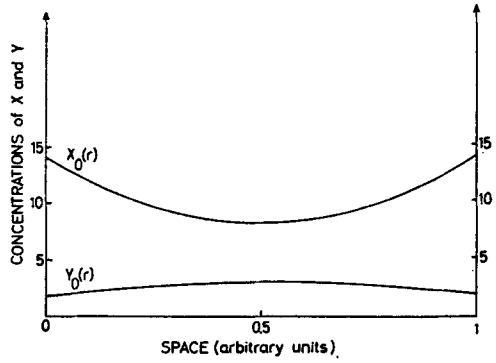

Figure 15. Steady state solution of (3.1) reducing to the 'thermodynamic' solution (1.5) in the limit of uniform distribution of A. The following numerical values have been chosen: $D_A = 1.972 \times 10^{-1}$, $D_X = 1.052 \times 10^{-3}$, $D_Y = 5.260 \times 10^{-3}$, $L = 1$, $B = 26$, $\bar{X} = \bar{A} = 14$, $\bar{Y} = B/\bar{A} = 1.86$

technique. The numerical results were obtained in the $B - D_Y$ plane for fixed values of $\bar{A}$, D_X and D_A (Herschkowitz-Kaufman and Platten, 1971; Herschkowitz-Kaufman, 1973), and define a stability diagram with three domains:

(1) a stable domain I, where all the real parts of the eigenvalues are negative.

(2) an unstable domain II, where at least one eigenvalue has a positive real part and a corresponding zero imaginary part.

(3) an unstable domain III, where at least one eigenvalue has a positive real part and a corresponding non zero imaginary part.

The results of this linear stability analysis and direct numerical integration of (3.1)–(3.3) agree very well.* The computer simulations show that:

in stable region I the initial perturbation dies out and the original steady state ($X_0(r)$, $Y_0(r)$) is restored;

for values of (B, D_Y) belonging to unstable region III the perturbations are

* For convenience the integration was performed by setting A at its steady state. This is justified by the fact that $A_0(r)$ is always stable and by the choice of $D_A \gg D_X$, D_Y which implies that concentration profile A relaxes very rapidly to A_0. The space $0 \leqslant r \leqslant L$ has now been divided in 156 equal space intervals defined by points 1–157.

amplified and a new, time periodic solution appears. This type of solution will be discussed elsewhere (see also Herschkowitz-Kaufman and Nicolis, 1972).

if the values of (B, D_Y) are above the neutral stability curve in region II, the system evolves to new steady states characterized by a space organization of X and Y similar to that observed in the 'homogeneous' case.

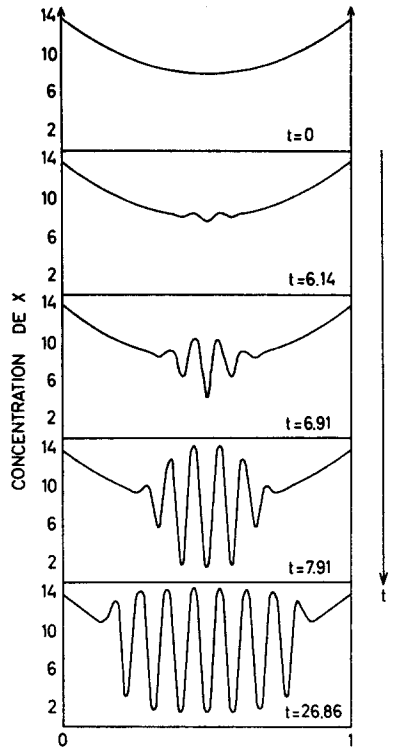

Figure 16. Time evolution towards a localized steady state dissipative structure arising beyond the point of instability of the 'generalized thermodynamic branch' $(X_0(r), Y_0(r))$. $B = 30$; other parameters are as in Figure 15

However, a new feature appears: the dissipative structure is localized in space (Figures 16–18). Depending on the values of intrinsical parameters such as B, D_Y, D_X, D_A, the system imposes its own limits to the organization. Within these *natural* borders one observes a regular spatial periodicity with short wavelength, while at the outside the concentration distribution is monotonous. Figure 16 illustrates the time evolution towards a localized structure. One sees the amplification of a fluctuation which extends progressively but never reaches the boundaries $r = 0$, $r = L$.

Properties

(a) *Localization.* Figures 17 and 18 illustrate the dependence of the localization effect on the parameters B and D_Y. One observes that the natural boundaries are displaced towards the limits $r = 0$ and $r = L$ as B increases and D_Y increases with respect to D_X.

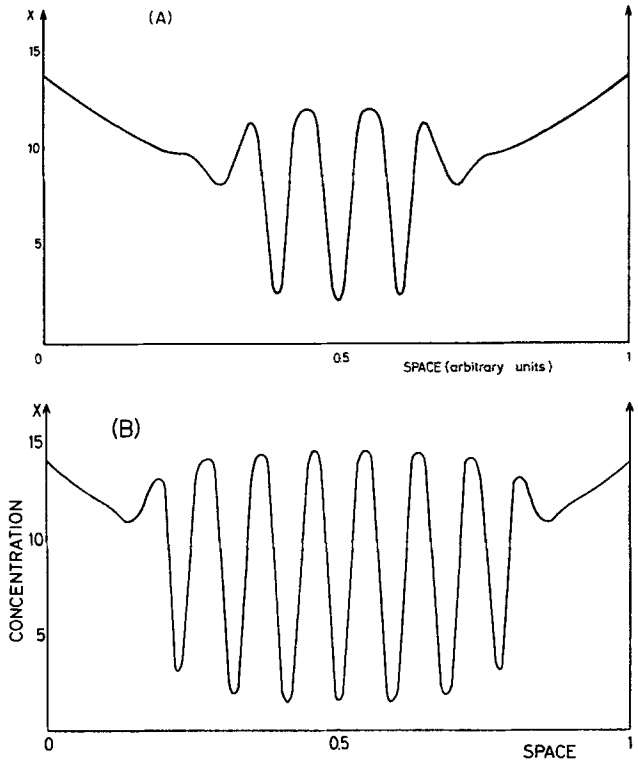

Figure 17. Localization of the dissipative structure in function of parameter B. Numerical values used: $D_A = 1.972 \times 10^{-1}$, $D_X = 1.052 \times 10^{-3}$, $D_Y = 5.260 \times 10^{-3}$, $L = 1$, $\bar{X} = \bar{A} = 14$. Figure 17A: $B = 24$, $\bar{Y} = B/\bar{A} = 1.71$. Figure 17B: $B = 30$, $\bar{Y} = B/\bar{A} = 2.14$

This localization effect is clearly due to the non uniform distribution of A which is maximum at the boundaries of the system (points 1 and 157) and minimum at the middle (point 79). A first estimate of this localization was given in the references by Herschkowitz-Kaufman and Nicolis (1972) and Herschkowitz-Kaufman (1973), on the basis of the linear stability analysis of the homogeneous steady state (1.5) which shows that instability arises when B

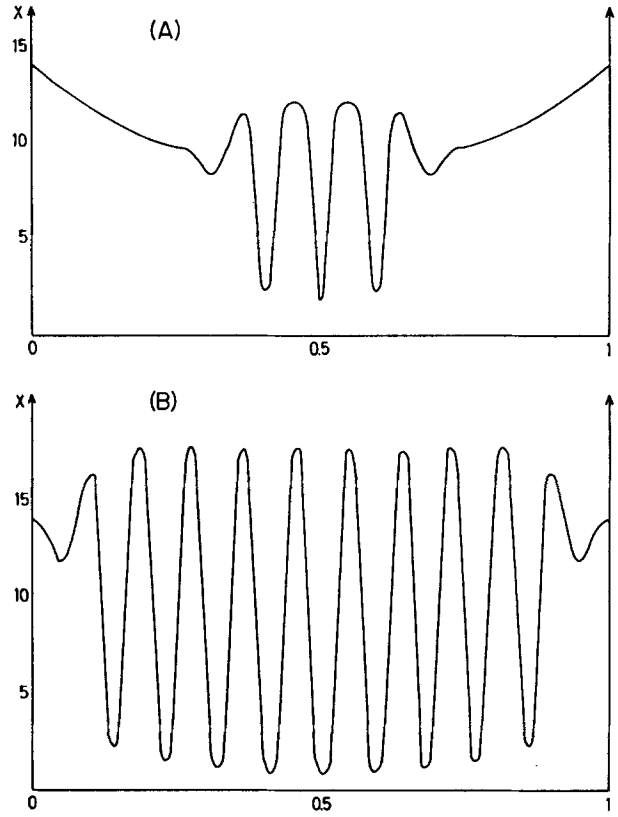

Figure 18. Localization of the dissipative structure in function of parameter D_Y. Numerical values used: $D_A = 1.972 \times 10^{-1}$, $D_X = 1.052 \times 10^{-3}$, $L = 1$, $B = 30$, $\bar{X} = \bar{A} = 14$, $\bar{Y} = B/\bar{A} = 2.14$. Figure 18A: $D_Y = 3.945 \times 10^{-3}$. Figure 18B: $D_Y = 7.890 \times 10^{-3}$

exceeds the critical value:

$$B_c = \left\{\left(\frac{D_X}{D_Y}\right)^{1/2} \cdot A + 1\right\}^2. \tag{3.5}$$

It follows that:

for $B > B_c^{\max} = B_c^{(1)} = B_c^{(157)}$, the structure will extend throughout the whole system;

for $B^{(79)} < B < B^{(157)}$ the dissipative structure region is normally localized and shrinks until it disappears for $B < B^{(79)}$.

The dependence on D_Y was explained in the same way. However this provides only a rough indication about the size of the oscillatory region. One observes

indeed that the spatial periodicity extends always further than predicted by the formula $B_c = \{(D_X/D_Y)^{1/2}A_0(r) + 1\}^2$. More recently, the localization of the dissipative structure within a defined portion of reaction space has been related by Auchmuty and Nicolis (1975) to the existence of turning points of the differential system (3.1). A comparison with their theoretical results is presented in the following section.

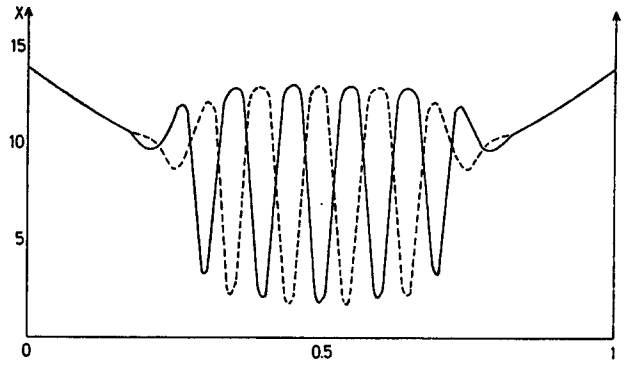

Figure 19. Degenerate localized dissipative structures obtained for the same values of the parameters but different initial conditions. Dashed line: initial perturbation: $\Delta X = +0.02$ at the middle point; Solid line: initial perturbation: $\Delta X = -0.02$ at the middle point. The parameters have the same numerical values as in Figure 15

(b) *Degeneracy, multiplicity.* Another characteristic feature is the dependence of the localized dissipative structures on the initial perturbation.

For perturbations of the same strength of the basic steady state $(X_0(r), Y_0(r))$ at a well defined point one obtains two entirely symmetrical dissipative structures depending on the sign of the perturbation. This is illustrated on Figure 19, for perturbations applied to the central point 79. This property is the same as the degeneracy observed for non localized dissipative structures.

The localization and wavelength of the structure seem not to depend on the location of the initial perturbation. Furthermore one observes that when the perturbation is applied near the boundaries of the system, it travels first towards the middle before being amplified.

When two perturbations are applied simultaneously one obtains either one of the two degenerate steady states or another similar solution which is in general asymmetric (Figure 20).

(c) *Duplication of the dissipative structure.* The nonlinear differential equations (3.1)–(3.2) were also numerically integrated for lower values of the diffu-

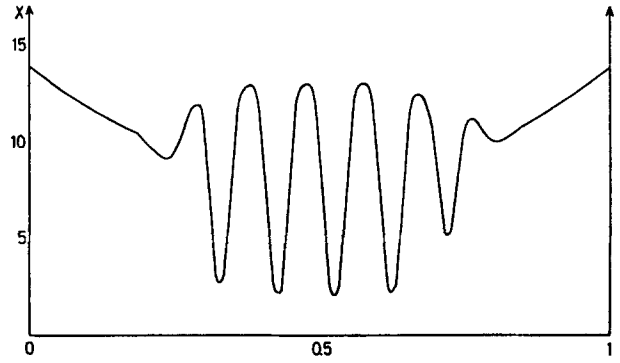

Figure 20. Localized dissipative structure obtained for the same numerical values of the parameters as in Figure 19. The initial condition consists now in two simultaneous perturbations of the basic steady state: $\Delta X = +0.02$ at point 64 and $\Delta X = -0.02$ at point 94

sion coefficient D_A which comes to impose a stronger non uniform constraint as in the preceeding examples (Figure 21A).

Figures 21B–D describe the spatial distribution of intermediate specie X in this case for some values of B.

Localization is always present but in addition one observes a very pronounced depression of X in the middle together with a duplication of the dissipative structure. The interpretation of this structure in terms of relation (3.5) is no more satisfactory.

In the framework of our computer simulations these concentration profiles seem to be independent of the location, amplitude and sign of the initial perturbation.

(d) *Wavelength.* The spatial organization inside the natural boundaries corresponds to a rapidly varying function of r.

Our numerical simulations for different values of B and D_Y seem to indicate that this short wavelength is only weakly dependent on the values of those parameters, while on the contrary they have a crucial action for the size of the spatial periodicity. Systematic variation of D_X was not carried.

On the other hand the amplitude of the extrema varies slightly with r and is the greatest near the middle, but always stays well within the limits determined by Auchmuty and Nicolis (1974).

2. Comparison Between Numerical and Theoretical Results

Auchmuty and Nicolis (1974) have undertaken a theoretical analysis of system (3.1) which leads to the interpretation of the localization of the dissipative

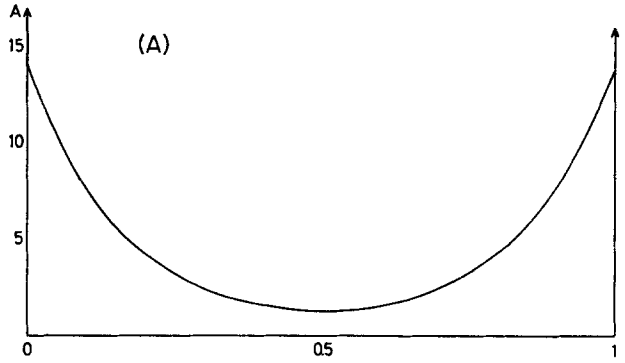
A
15
10
5
(A)
0
0.5
1

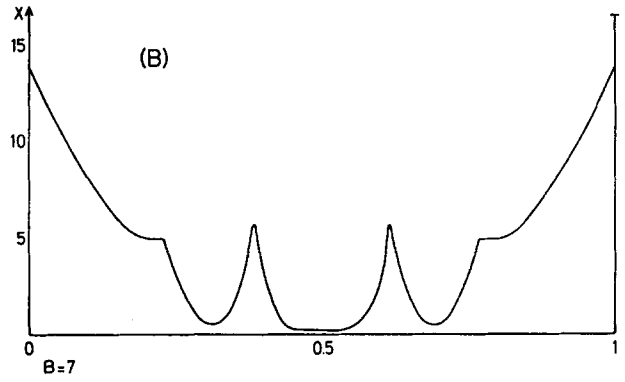
X
15
10
5
(B)
0
0.5
1
B=7

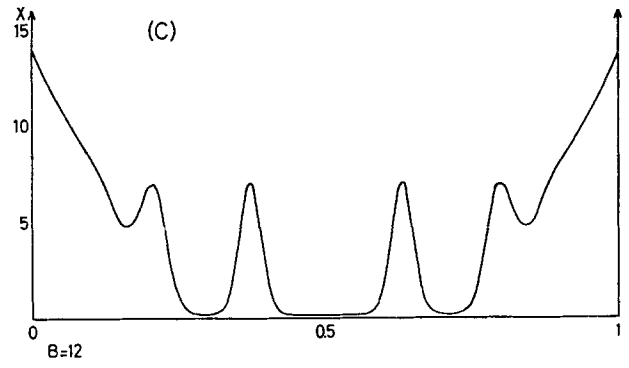
X
15
10
5
(C)
0
0.5
1
B=12

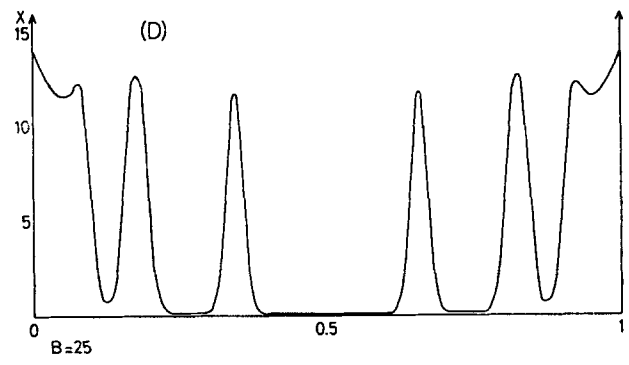
X
15
10
5
(D)
0
0.5
1
B=25

structure in terms of turning points of the differential system. These turning points determine the boundaries between two types of behavior in space: monotonic and oscillatory. We summarize their principal results. To investigate the existence of a steady state solution of dissipative structure type one introduces in equations (3.1) taken at the steady state:

$$\begin{aligned} X(r) &= X_0(r) + x(r) \\ Y(r) &= Y_0(r) + y(r) \\ |x/X_0| \ll 1, &\qquad |y/Y_0| \ll 1 \end{aligned} \tag{3.6}$$

and seeks for non zero solutions of the linearized equations for x and y. The basic steady state $(X_0(r), Y_0(r))$ is approximated by a power series in $1/D_A$, in the limit of small D_X/D_A, D_Y/D_A and large D_A.

Introducing the new variable $z = D_X x + D_Y y$, the linear set of equations for x and y can be written as a single fourth order equation:

$$D_X \cdot \frac{d^4 z}{dr^4} + [F(r) - \tfrac{1}{2}(B_+(r) + B_-(r)]\frac{d^2 z}{dr^2} + \frac{1}{D_Y} X_0^2(r) z = 0 \tag{3.7}$$

where:

$$F(r) = 2X_0(r)Y_0(r) - B \tag{3.8}$$

$$B_\pm(r) = \left[\left(\frac{D_X}{D_Y}\right)^{1/2} X_0(r) \pm 1\right]^2. \tag{3.9}$$

Nicolis and Auchmuty have shown (in the limit of large D_A) that this equation can admit two turning points.

Indeed, the solution $z(r)$ will be monotonic in certain regions of space provided the following conditions can be satisfied:

$$F(r) \leqslant 1 + \frac{D_X}{D_Y} \cdot X_0^2(r) \tag{3.10}$$

$$F(r) \leqslant B_-(r). \tag{3.11}$$

Elsewhere $z(r)$ will be oscillatory in space. The turning points (r_{01}, r_{02}) separating these two types of behavior are defined by:

$$2X_0(r)Y_0(r) - B = B_-(r). \tag{3.12}$$

Figure 21. (A): steady state profile of A for $\bar{A} = 14$, $D_A = 2.60 \times 10^{-2}$. (B–D): Spatial distribution of X corresponding to the 'duplication' of the steady state dissipative structure. Numerical values used: $D_A = 2.60 \times 10^{-2}$, $D_X = 1.052 \times 10^{-3}$, $D_Y = 5.260 \times 10^{-3}$, $\bar{X} = \bar{A} = 14$, $L = 1$. B is respectively equal to 7, 12 and 25. $(\bar{Y} = B/\bar{A})$

When $F(r) \geqslant B_+(r)$ in the entire interval $(0, L)$, (3.10) is always contradicted so that turning points cannot be defined and the dissipative structure should in principle be entirely delocalized.

Nicolis and Auchmuty have more specially investigated the case where the functions $B_\pm(r)$ vary slowly on $[0, L]$ and $F(r) \simeq B$, which is represented schematically in Figure 22.

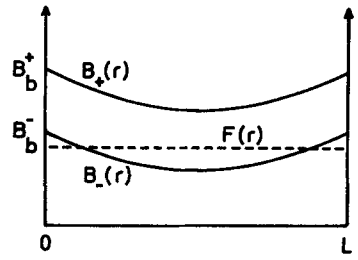

Figure 22

They have shown that in the neighborhood of the turning points one obtains:

$$z(r) \sim \exp\{i \cdot \text{const.} \, |r - r_{0i}|^{3/2}\} \tag{3.13}$$

which is non sinusoidal; whereas near the middle point $r = \frac{1}{2}$:

$$z(r) \sim \exp\{i \cdot \text{const.} \, (r - \tfrac{1}{2})\} \tag{3.14}$$

which is approximately sinusoidal.

Furthermore, their analysis indicates that the turning points r_{01}, r_{02} are displaced towards the boundaries $r = 0$, $r = L$:

(1) as B increases and tends to the critical value $B_b = \{\bar{A}(D_X/D_Y)^{1/2} + 1\}^2$, for which the dissipative structure becomes entirely delocalized;
(2) for increasing values of $\lambda = \bar{A} \cdot (D_X/D_Y)^{1/2}$ whenever the function:

$$f(\lambda) = \frac{1}{\lambda} \cdot \left\{1 - \frac{B}{(\lambda - 1)^2}\right\}$$

is a decreasing function of λ, which is the case for large λ.

These results might be compared with the computer results presented in this chapter. However, the theoretical calculations provide only very rough information on the localized dissipative structures as they apply principally to the case of D_A very large. This implies that $A(r)$ and the generalized thermodynamic solution $(X_0(r), Y_0(r))$ correspond to very flat concentration profiles. This is not the case for our numerical results so that $B_\pm(r)$ vary considerably in interval $(0, L)$ and the condition $F(r) < B_+(r)$ is never satisfied for all r. The situations which correspond to our numerical results are illustrated in

Figure 23 for two characteristic examples, by using for $(X_0(r), Y_0(r))$ the approximated solutions obtained by the local potential technique.

Case 1: Figure 23A: $B < B_b^- = \{\bar{A} \cdot (D_X/D_Y)^{1/2} - 1\}^2$ (see for example Figures 17A and 18B).

Comparing the theoretical predictions with the localized dissipative structures

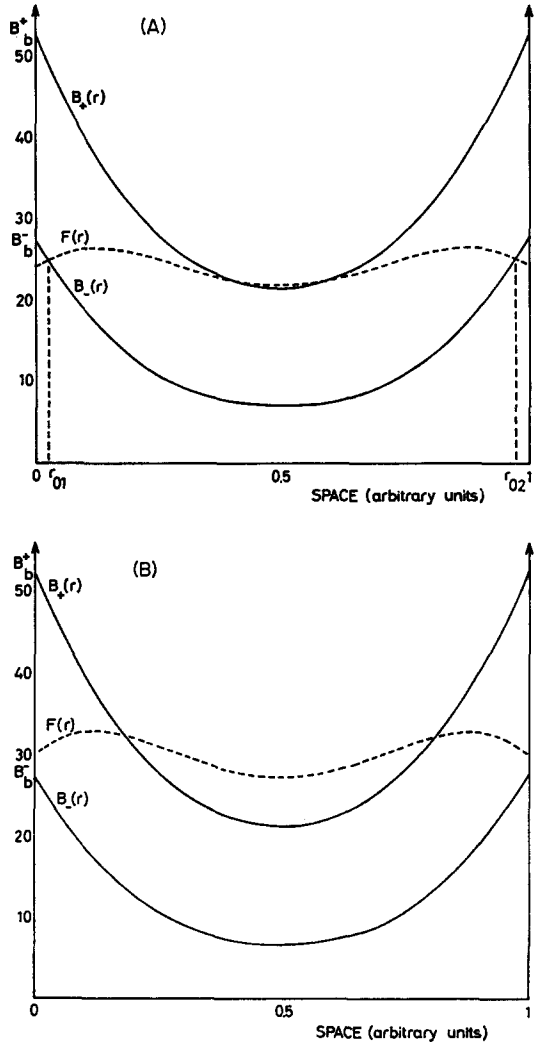

Figure 23. B^+, B^- and F given by formulae (3.8) and (3.9) are plotted against r for two values of B. The numerical values of the parameters are the same as in Figure 17. Figure 23A: $B = 24$. Figure 23B: $B = 30$

obtained by computer simulation, one observes that in spite of the fact that $z(r)$ should be oscillatory inside (r_{01}, r_{02}) determined by (3.12) the size of the dissipative structure is much smaller than predicted. This could be explained by the fact that the wavelength of the oscillatory solution (3.14) varies with r in such a way that the oscillations appear negligible near the turning points (3.12). The periodic behavior is not however limited to the interval defined by $F(r) = B_+(r)$. This is to be compared with the qualitative estimation presented in Section III.1(a).

Case 2: Figure 23B: $B > B_b^- = \{\bar{A} \cdot (D_X/D_Y)^{1/2} - 1\}^2$ (see for example Figures 17B and 18B)

While the theoretical calculations predict an entirely delocalized dissipative structure one observes from the numerical calculations that the solution is apparently not necessarily oscillatory near the boundaries but again is not confined within the limits $F(r) = B_+(r)$.

As before this could be explained by the non uniformity of the wavelength so that the oscillations behave differently near the boundaries (long wavelength) and near the middle (short wavelength). As a result the solution appears non oscillatory near the boundaries.

In the case of very low values of the diffusion coefficient D_A as considered in Figure 21, extension of the theoretical calculations will presumably lead to the appearance of additional turning points which separate the two dissipative structure regions. Indeed since in this case $F(r)$ can vary considerably in space, the observed depression in the middle could correspond to the situation $F(r) < B_-(r)$ around $r = L/2$, which corresponds to a non oscillatory behavior. This point is under investigation.

In conclusion, one sees that the introduction of a dispersive medium leads to a great variety of situations. A better understanding of the exact location of the boundaries of the dissipative structures requires an extension of the theoretical calculations with higher order terms and a careful study of the behavior in space of the wavelength of the oscillatory solutions as a function of the system's parameters.

I wish to express my gratitude to Prof. I. Prigogine and Prof. G. Nicolis for their interest in this work and stimulating discussions. I further thank Prof. J. F. G. Auchmuty and Prof. P. Glansdorff for continuous encouragement and advice. This research has been supported by the Fonds de la Recherche Fondamentale Collective.

LITERATURE

Auchmuty, J. F. G. and G. Nicolis. 1974. "Bifurcation Analysis of Nonlinear Reaction-Diffusion Equations–I." *Bull. Math. Biol.*, **37**, 1–43.

Babloyantz, A. and J. Hiernaux. 1974. "Models for Positional Information and Positional Differentiation." *Proc. Nat. Acad. Sci., U.S.A.*, **71**, 1530–1533.

Chance, B., K. Pye, A. K. Ghosh and B. Hess. 1973. *Biological and Biochemical Oscillators*. New York: Academic Press.

Erneux, T. and M. Herschkowitz-Kaufman. 1975. "Dissipative Structures in Two Dimensions." *Biophys. Chem.* In press.

Glansdorff, P. and I. Prigogine. 1971. *Thermodynamics of Structure, Stability and Fluctuations*. New York: Wiley–Interscience.

Goldbeter, A. and R. Lefever. 1972. "Dissipative Structures for an Allosteric Model—Application to Glycolitic Oscillations." *Biophys. J.*, **12**, 1302–1315.

Hanson, M. P. 1974. "Spatial Structures in Dissipative Systems." *J. Chem. Phys.*, **60**, 3210–3214.

Hanusse, P. 1972. "De l'Existence d'un Cycle Limite dans l'Evolution des Systèmes Chimiques Ouverts." *C. R. Acad. Sci. Paris*, **C274**, 1245–1247.

Herschkowitz-Kaufman, M. and J. K. Platten. 1971. "Chemical Instabilities and Localized Structures in non Homogeneous Media." *Bull. Cl. Sci. Acad. Roy. Belg.*, **57**, 26–40.

——— and G. Nicolis. 1972. "Localized Spatial Structures and Nonlinear Chemical Waves in Dissipative Systems." *J. Chem. Phys.*, **56**, 1890–1895.

———. 1973. "Quelques Aspects du Comportement de Systèmes Chimiques Ouverts loin de l'Equilibre Thermodynamique." Ph. D. Thesis, Université Libre de Bruxelles, Belgium.

Kopell, N. and L. N. Howard. 1973. "Horizontal Bands in the Belousov Reaction." *Science*, **180**, 1171–1173.

——— and ———. 1973. "Plane Wave Solutions to Reaction Diffusion Equations." *Stud. appl. Math.*, **52**, 291.

Martinez, H. 1972. "Morphogenesis and Chemical Dissipative Structures." *J. Theor. Biol.*, **36**, 479–501.

Nicolis, G. and J. F. G. Auchmuty. 1974. "Dissipative Structures, Catastrophes and Pattern Formation: A Bifurcation Analysis." *Proc. Nar. Acad. Sci., U.S.A.*, **71**, 2748–2751.

——— and J. Portnow. 1973. "Chemical Oscillations." *Chem. Rev.*, **73**, 365–384.

Nitzan, A., P. Ortoleva and J. Ross. 1974. "Symmetry Breaking Instabilities in Illuminated Systems." *J. Chem. Phys.*, **60**, 3134–3143.

Noyes, R. M., R. J. Field and E. Körös. 1972. "Oscillations in Chemical Systems—I. Detailed Mechanism in a System Showing Temporal Oscillations." *J. Amer. Soc.*, **95**, 1394–1395.

——— and ———. 1974. "Oscillatory Chemical Reactions." *Ann. Rev. Phys. Chem.*, **25**, to appear.

Ortoleva, P. and J. Ross. 1974. "On a Variety of Wave Phenomena in Chemical Reactions." *J. Chem. Phys.*, **60**, 5090–5107.

Perlmutter, D. 1972. *The Stability of Chemical Reactions*. Englewood Cliffs, N.J: Prentice Hall.

Prigogine, I. 1969. "Structure, Dissipation and Life." In *Theoretical Physics and Biology*, Ed. M. Marois, p. 23. Amsterdam: North Holland.

——— and G. Nicolis. 1971. "Biological Order, Structure and Instabilities." *Rev. Biophys.*, **2**, **3**, and **4**, 107–148.

Sattinger, D. 1973. "Topics in Stability and Bifurcation Theory." *Lecture Notes in Mathematics*, Vol. 309. Berlin: Springer.

Turing, A. M. 1952. "The Chemical Basis of Morphogenesis." *Phil. Trans. Roy. Soc. (Lond.)*, **237B**, 37–72.

Tyson, J. 1973. "Some Further Studies of Nonlinear Oscillations in Chemical Systems." *J. Chem. Phys.*, **58**, 3919–3930.

——— and J. Light. 1973. "Properties of Two-component Bimolecular and Trimolecular Chemical Reaction Systems." *Ibid.*, **59**, 4164–4173.

Winfree, A. T. 1974. "Wavelike Activity in Biological and Chemical Media." In *Lecture Notes in Biomathematics* (Ed. P. van den Driessche) Berlin: Springer (in press).

RECEIVED 1-7-75
REVISED 5-28-75